# Ambient Conversion of CO<sub>2</sub> to Hydrocarbons by Biogenic and Synthetic [Fe<sub>4</sub>S<sub>4</sub>] Clusters

Martin T. Stiebritz,<sup>1,a</sup> Caleb J. Hiller,<sup>1,2,a</sup> Nathaniel S. Sickerman,<sup>1,a</sup> Chi Chung Lee,<sup>1,a</sup> Kazuki Tanifuji,<sup>1</sup> Yasuhiro Ohki<sup>3</sup> & Yilin Hu<sup>1,\*</sup>

<sup>1</sup>Department of Molecular Biology and Biochemistry, University of California, Irvine, CA 92697-3900; <sup>2</sup>Department of Chemistry, University of California, Irvine, CA 92697-2025; <sup>3</sup>Department of Chemistry, Graduate School of Science, Nagoya University, Furo-cho, Chikusa-ku, Nagoya, 464-8602, Japan.

<sup>&</sup>lt;sup>a</sup>These authors contributed equally to this work.

<sup>\*</sup>Correspondence should be addressed to <a href="mailto:yilinh@uci.edu">yilinh@uci.edu</a>.

#### **Abstract:**

The Fe protein of nitrogenase contains a redox active [Fe<sub>4</sub>S<sub>4</sub>] cluster that plays a key role in electron transfer and substrate reduction. Here we show that the Fe protein of *Methanosarcina acetivorans* can reduce CO<sub>2</sub> and CO to hydrocarbons under ambient conditions. Further, we demonstrate that this reactivity is inherent to [Fe<sub>4</sub>S<sub>4</sub>] clusters, showing the ability of a synthetic [Fe<sub>4</sub>S<sub>4</sub>] compound to catalyse the same ambient reaction in solutions. Theoretical calculations suggest a reaction mechanism involving an aldehyde-like intermediate that gives rise to hydrocarbon products upon proton-coupled electron transfer and concomitant removal of water molecules. These results provide a framework for mechanistic investigations of FeS-based activation and reduction of CO<sub>2</sub> and CO while facilitating potential development of FeS catalysts capable of ambient conversion of CO<sub>2</sub> and CO into fuel products.

Iron-sulphur (FeS) proteins are crucial for a wide variety of biological functions, such as electron transfer, enzyme catalysis, iron homeostasis, DNA synthesis, and gene regulation<sup>1-5</sup>. Designated the iron (Fe) protein, the reductase component of nitrogenase is a homodimeric protein containing a subunit-bridging [Fe<sub>4</sub>S<sub>4</sub>] cluster<sup>6-8</sup>, and it serves as an obligate electron donor for its catalytic partner during catalysis. Recently, the Fe protein of Azotobacter vinelandii, a soil bacterium, was shown to act as a reductase on its own and catalyse the ambient reduction of CO<sub>2</sub> to CO under in vitro or in vivo conditions via the redox change of its [Fe<sub>4</sub>S<sub>4</sub>] centre; however, further reduction past CO was not detected in this case<sup>9</sup>. This observation has piqued our interest in further exploring the reactivity of the nitrogenase Fe protein toward CO<sub>2</sub> and addressing the question of whether the Fe protein can reduce CO<sub>2</sub> beyond CO into hydrocarbon products. The Fe protein homologs from methanogenic organisms are interesting subjects of study along this line of pursuit, given the high concentration of CO<sub>2</sub> in the habitat of these organisms and their metabolic adaptation to CO<sub>2</sub> reduction. Moreover, the relatively surface-exposed location of the [Fe<sub>4</sub>S<sub>4</sub>] cluster in the Fe protein<sup>6-8</sup> points to the possibility that [Fe<sub>4</sub>S<sub>4</sub>] clusters that exist freely in solutions may have the same CO<sub>2</sub>-reducing activity as their protein-bound counterpart. Understanding the reactivity of the [Fe<sub>4</sub>S<sub>4</sub>] cluster toward CO<sub>2</sub> is important, as it would enable identification of simple FeS clusters as catalysts that mimic the function of the industrial Fischer-Tropsch process<sup>10</sup> in carbon fuel production under ambient conditions.

Here we show that the Fe protein of *Methanosarcina acetivorans* is capable of ambient reduction of CO<sub>2</sub> and CO to hydrocarbons. We further demonstrate that this reactivity is inherent to [Fe<sub>4</sub>S<sub>4</sub>] clusters, as a synthetic [Fe<sub>4</sub>S<sub>4</sub>] compound can catalyse the same reaction in solutions. Our theoretical calculations suggest a reaction mechanism involving an aldehyde-like intermediate,

thereby providing a useful framework for mechanistic investigations of FeS-based CO<sub>2</sub> reduction and future development of strategies to recycle CO<sub>2</sub> into valuable chemical commodities.

#### **Results**

Reduction of CO<sub>2</sub> and CO by protein-bound [Fe<sub>4</sub>S<sub>4</sub>] clusters. To examine the reactivity of methanogen Fe proteins toward CO<sub>2</sub>, we expressed the Fe protein of Methanosarcina acetivorans in Escherichia coli<sup>11</sup> and conducted comparative CO<sub>2</sub> reduction assays of this Fe protein with the Fe protein of A. vinelandii. Like its A. vinelandii counterpart (designated NifH $^{Av}$ ), the Fe protein of M. acetivorans (designated NifH $^{Ma}$ ) was capable of reducing  $CO_2$  to CO in the presence of a strong reductant, europium diethylenetriaminepentaacetic acid (Eu<sup>II</sup>-DTPA;  $E^{0'}$  = -1.14 V at pH 8)<sup>12</sup>. In the case of NifH<sup>Av</sup>, the yield of CO increased when the concentration of Eu<sup>II</sup>-DTPA was increased from 10 to 100 mM (Fig. 1a). In the case of Nifh $^{Ma}$ , however, while the formation of CO increased slightly upon an increase of the concentration of Eul-DTPA from 10 to 20 mM, it decreased concomitantly with an increase in the formation of C<sub>1</sub>-C<sub>3</sub> hydrocarbons when Eu<sup>II</sup>–DTPA concentration was increased beyond 20 mM, reaching a maximum hydrocarbon yield of 3.9 nmol reduced C/nmol cluster at 100 mM Eu<sup>II</sup>-DTPA (Fig. 1a). Gas chromatography-mass spectrometry (GC-MS) analysis further confirmed that these hydrocarbon products originated from CO<sub>2</sub>, showing the characteristic fragmentation patterns and expected mass shifts of C<sub>1</sub> (CH<sub>4</sub>), C<sub>2</sub> (C<sub>2</sub>H<sub>4</sub>, C<sub>2</sub>H<sub>6</sub>) and C<sub>3</sub> (C<sub>3</sub>H<sub>6</sub>, C<sub>3</sub>H<sub>8</sub>) products by +1, +2 and +3, respectively, upon substitution of <sup>13</sup>CO<sub>2</sub> for <sup>12</sup>CO<sub>2</sub> (Fig. 1b). Interestingly, despite an increase in the hydrocarbon/CO ratio with increasing concentrations of Eu<sup>II</sup>–DTPA, the total carbon yield calculated on the basis of both CO and hydrocarbons remained approximately the same (~5 nmol reduced C/nmol cluster) when ≥20 mM Eu<sup>II</sup>–DTPA was supplied to the NifH<sup>Ma</sup>-catalysed reaction (Fig. 1a), suggesting a reductant concentration-dependent re-distribution of electrons between COand hydrocarbon-formation in the NifH $^{Ma}$ -catalysed reaction (Supplementary Fig. 1). In contrast,

hydrocarbon products could not be detected in the NifH<sup>Av</sup>-catalysed reaction (Fig. 1a), highlighting the difference between NifH<sup>Av</sup> and NifH<sup>Av</sup> in their reactivities toward CO<sub>2</sub>.

The same discrepancy between NifH $^{Ma}$  and NifH $^{Av}$  was observed when CO was supplied as a substrate, as  $C_1$ - $C_4$  hydrocarbons were only detected in the reaction catalysed by NifH<sup>Ma</sup> (Fig. 1c). The reduction of CO to hydrocarbons by NifH<sup>Ma</sup>, like that of CO<sub>2</sub> to hydrocarbons, increased dramatically with increasing Eu<sup>II</sup>– DTPA concentrations, reaching a maximum turnover number (TON) of 29.5 at 100 mM Eu<sup>II</sup>-DTPA (Fig. 1c). GC-MS analysis provided evidence that these hydrocarbons were derived from the substrate CO, showing the expected fragmentation patterns and mass shifts of the C<sub>1</sub> (CH<sub>4</sub>), C<sub>2</sub> (C<sub>2</sub>H<sub>4</sub>, C<sub>2</sub>H<sub>6</sub>), C<sub>3</sub> (C<sub>3</sub>H<sub>6</sub>, C<sub>3</sub>H<sub>8</sub>) and C<sub>4</sub> (C<sub>4</sub>H<sub>8</sub>, C<sub>4</sub>H<sub>10</sub>) products when <sup>12</sup>CO was replaced by <sup>13</sup>CO (Fig. 1d). Notably, the TONs of the reactions of COreduction were consistently higher than those of the reactions of CO<sub>2</sub>-reduction at varying concentrations of Eu<sup>II</sup>–DTPA, with the biggest difference between the two (by 7.5-fold) observed at 100 mM Eu<sup>II</sup>–DTPA (Fig. 2a, b). Moreover, there was a shift toward formation of longer hydrocarbon chains when COreduction was compared with CO<sub>2</sub>-reduction, although both reactions showed a tendency toward formation of longer hydrocarbon products with increasing concentrations of Eu<sup>II</sup>-DTPA (Fig. 2a, b). Despite these differences, the reduction of CO and CO<sub>2</sub> by NifH<sup>Ma</sup> displayed similar hydrocarbon product distributions (Fig. 2a, b), suggesting routing of the reduction of CO<sub>2</sub> via CO or CO-derived intermediates. It is plausible, therefore, that the differential reactivities of NifH<sup>Ma</sup> and NifH<sup>Av</sup> toward CO<sub>2</sub> originate from differential binding affinities of these proteins to the intermediate CO, with NifH<sup>Ma</sup> having a much stronger affinity for CO than NifH<sup>Av</sup>, which facilitates the reduction of CO and formation of C-C bonds by NifH<sup>Ma</sup> while permitting the release of CO as an end product by NifH<sup>Av</sup>. The observation that the product yield of NifH<sup>Ma</sup> saturated quickly (at  $\sim 0.5\%$  CO) with increasing CO concentrations provides support for a high affinity of NifHMa for CO (Supplementary Fig. 2). Additionally, the ability of the oxidized NifH $^{Av}$  to catalyse the conversion

of CO to  $CO_2^9$ —a feature resembling the  $CO/CO_2$  interconverting enzyme, carbon monoxide dehydrogenase<sup>13-15</sup>—was not duplicated in the case of the oxidized NifH<sup>Ma</sup> (Supplementary Fig. 3a), which could further contribute to the differential reactivities of these two Fe proteins toward CO and  $CO_2$ . Such a difference likely reflects a difference in the redox potentials of NifH<sup>Ma</sup> and NifH<sup>Av</sup>, with the [Fe<sub>4</sub>S<sub>4</sub>]<sup>1+/2+</sup> couple of the former protein ( $E^0$ ' = –395 mV) showing a significantly lower redox potential than that of the latter protein ( $E^0$ ' = –301 mV) (Supplementary Fig. 3b, c). Indeed, when driven by 200 mM dithionite ( $E^0$ ' ≈ –430 mV at pH 7)<sup>16</sup>, NifH<sup>Ma</sup> was capable of reducing CO to hydrocarbons at low yields, with a product profile resembling that generated in the presence of Eu<sup>II</sup>–DTPA; whereas no hydrocarbon could be detected in the reaction catalysed by NifH<sup>Av</sup> under the same conditions (Supplementary Fig. 4a, b). Importantly, the fact that CO can be reduced by NifH<sup>Ma</sup> at a redox potential mimicking that in the cell suggests a potential physiological relevance of this reaction.

Reduction of CO<sub>2</sub> and CO by synthetic [Fe<sub>4</sub>S<sub>4</sub>] clusters. The observation of ambient conversion of CO<sub>2</sub> and CO to hydrocarbons by a protein-bound [Fe<sub>4</sub>S<sub>4</sub>] cluster (Supplementary Fig. 5a) has led to the question of whether the reactivity toward these substrates is an inherent catalytic feature of the [Fe<sub>4</sub>S<sub>4</sub>] clusters. To address this question, a synthetic [PPh<sub>4</sub>][Fe<sub>4</sub>S<sub>4</sub>(SCH<sub>2</sub>CH<sub>2</sub>OH)<sub>4</sub>] compound (designated [Fe<sub>4</sub>S<sub>4</sub>]<sup>Syn</sup>) containing a [Fe<sub>4</sub>S<sub>4</sub>] core and four cysteine-like, β-mercaptoethanol (BME) thiolate ligands (Supplementary Fig. 5b)<sup>17,18</sup>, was tested for its ability to reduce CO<sub>2</sub> and CO. Driven by 20 mM Eu<sup>II</sup>–DTPA in an aqueous buffer, [Fe<sub>4</sub>S<sub>4</sub>]<sup>Syn</sup> was capable of generating up to C<sub>2</sub> hydrocarbon products (i.e., CH<sub>4</sub>, C<sub>2</sub>H<sub>4</sub>, C<sub>2</sub>H<sub>6</sub>) hydrocarbons at TONs of 0.3 and 0.4, respectively, in the reactions of CO<sub>2</sub>- and CO-reduction (Fig. 2a, b). Substitution of 20 mM samarium(II) iodide (SmI<sub>2</sub>;  $E^{0}$ , ≈ −1.5 V in DMF)<sup>19</sup> along with a proton source, triethyl-

ammonium tetrafluoroborate [Et<sub>3</sub>NH(BF<sub>4</sub>)], in the organic solvent dimethylformamide (DMF) for Eu<sup>II</sup>–DTPA in an aqueous buffer resulted in substantial increases of hydrocarbon formation to TONs of 15.8 and 89.7, respectively, in the [Fe<sub>4</sub>S<sub>4</sub>]<sup>Syn</sup>–catalysed reactions of CO<sub>2</sub>- and CO-reduction while pushing both reactions toward the formation of up to C<sub>4</sub> hydrocarbon products (i.e., CH<sub>4</sub>, C<sub>2</sub>H<sub>4</sub>, C<sub>2</sub>H<sub>6</sub>, C<sub>3</sub>H<sub>6</sub>, C<sub>3</sub>H<sub>8</sub>, C<sub>4</sub>H<sub>8</sub>, C<sub>4</sub>H<sub>10</sub>) (Fig. 2a, b). Remarkably, the maximum TONs of [Fe<sub>4</sub>S<sub>4</sub>]<sup>Syn</sup> in the reactions of CO<sub>2</sub>- and CO-reduction were 4- and 3-fold, respectively, of those of the biogenic [Fe<sub>4</sub>S<sub>4</sub>] cluster in NifH<sup>Ma</sup> (Fig. 2a, b), likely due to the improved accessibility of the reaction site in solutions of [Fe<sub>4</sub>S<sub>4</sub>]<sup>Syn</sup> clusters that increased the overall yields of hydrocarbons in the reactions of CO<sub>2</sub>- and CO-reduction. Compared to the activity of hydrocarbon formation by [Fe<sub>4</sub>S<sub>4</sub>]<sup>Syn</sup>, the CO<sub>2</sub>- and CO-reducing activities of iron(III) chloride (FeCl<sub>3</sub>) solutions containing equimolar Fe to that of the [Fe<sub>4</sub>S<sub>4</sub>]<sup>Syn</sup> cluster were only 7% and 4%, respectively, in the presence of sodium sulphide (Na<sub>2</sub>S); and 2% and 2%, respectively, in the absence of Na<sub>2</sub>S (Supplementary Fig. 6a, b), providing strong, albeit indirect proof that the activity of [Fe<sub>4</sub>S<sub>4</sub>]<sup>Syn</sup> did not originate from small Fe/S fragments/constituents.

Proposed pathway of CO<sub>2</sub> reduction by the [Fe<sub>4</sub>S<sub>4</sub>] cluster. Density functional theory (DFT) calculations, which provided mechanistic insights into the reaction of CO reduction by vanadium nitrogenase<sup>20</sup>, were performed on the [Fe<sub>4</sub>S<sub>4</sub>] cluster, leading to the proposal of plausible mechanisms of [Fe<sub>4</sub>S<sub>4</sub>]-cluster-catalysed CO<sub>2</sub>/CO reduction (see Methods and Supplementary Notes 1-3; also see Supplementary Fig. 7). One mechanism involves protonation and dissociation of a thiolate ligand, which permits C-C coupling at the same Fe centre of the cluster (Fig. 3; also see Supplementary Figs. 8a and 9a). Binding of CO<sub>2</sub> to the cluster is only slightly exothermic (Fig. 3a, step 1), which might contribute to the moderate turnover efficiency of this catalyst. Favourable coordination of

CO<sub>2</sub> to one Fe atom of the free cluster, like that observed in the case of the protein-bound cluster<sup>9</sup>, occurs when the cluster is present in the all-ferrous oxidation state with a S=0 spin state (Supplementary Note 3). Protonation of the coordinated CO<sub>2</sub> species, followed by proton-coupled electron transfer, then initiates cleavage of a water molecule and leaves the cluster in a CO-bound, [Fe<sub>4</sub>S<sub>4</sub>]<sup>+</sup> state (Fig. 3a, steps 2, 3). The reaction pathway becomes branched at this point. In one branch, the reaction continues with dissociation of CO (Fig. 3a, step 4) and re-reduction of the cluster (Fig. 3a, step 5). Dissociation of CO is energetically disfavoured, as is the re-reduction of the cluster, which is consistent with the low CO<sub>2</sub>-reducing activity of the cluster. In the other branch, the reaction proceeds with protonation-induced dissociation of the thiolate ligand at the Fe atom coordinated by CO (Fig. 3b, step 6), followed by proton-coupled electron transfer to the Fecoordinated CO moiety, forming an aldehyde-like, iron-formyl species (Fig. 3b, step 7). Subsequently, this moiety could undergo an overall exothermic series of proton-coupled electron transfer steps (see Supplementary Fig. 9a), which, coupled with dissociation of a water molecule, eventually lead to a reactive cluster-bound CH<sub>3</sub> group (Fig. 3b, steps 8-11). Subsequent electron transfer and proton transfer from a free thiol molecule readily yield CH4 and restore the cluster to its fully thioethanolate-coordinated form (Fig. 3b, step 12).

Several mechanistic branching points are possible that involve coordination of a second CO molecule when a primary C<sub>1</sub> species is still bound to the cluster. One likely pathway for C-C bond formation involves coordination of CO at the CH<sub>3</sub>-bound Fe site, which is exothermic by ca. -14 kcal/mol and allows for an exothermic migratory insertion, yielding an iron-acetyl intermediate (Fig. 3c, steps 14, 15). A subsequent series of reduction and proton-transfer steps, which is overall highly exothermic (see Supplementary Fig. 9a), results in dissociation of a water molecule and formation of an Fe-bound ethyl moiety (Fig. 3c, steps 15-19). Note that, for the dissociation of

water to occur, the cluster has to be formally present in the all-ferrous [Fe<sub>4</sub>S<sub>4</sub>]<sup>0</sup> state (Fig. 3c, step 18, transfer of two electrons). Subsequent exothermic proton-coupled electron transfer readily yields a cluster-bound ethyl species (Fig. 3c, steps 17, 18). Analogous to the formation of the C<sub>1</sub> species, 'recombination' of the cluster with a thiol molecule results in the formation of C<sub>2</sub>H<sub>6</sub> (Fig. 3c, step 19), and restores the cluster to the [Fe<sub>4</sub>S<sub>4</sub>]<sup>0</sup> or [Fe<sub>4</sub>S<sub>4</sub>]<sup>+</sup> state, depending on whether an additional electron is simultaneously transferred (Fig. 3c, steps 20a, 20b). It seems energetically plausible for the cluster to employ a similar mechanism for the formation of longer carbon chains: CO could coordinate to an ethyl-bound Fe atom with a reaction energy of ca. –12 kcal/mol, followed by another round of migratory insertion, which would be exothermic by ca. –9 kcal/mol. Due to multiple competing reaction branches, however, the probability for this chain elongation event to occur would be substantially lower than for the C<sub>2</sub> mechanism (e.g., dissociation of the carbon species), which is in line with the experimentally observed bias toward short-chain product formation (Fig. 2).

Other than the mechanism proposed above, which involves removal of the thiolate ligand (Fig. 3a, step 6) for the subsequent C-C coupling via migratory insertion at a single Fe site (Fig. 3c, step 14), an alternative mechanism is conceivable for the fully ligated cluster, which allows the pathway to proceed through coordination events at two neighbouring Fe centres (Fig. 4; Supplementary Figs. 8b and 9b). The two mechanisms share the same pathway for CO reduction (Figs. 3a and 4a, steps 1-5) and analogous pathways for CH<sub>4</sub> formation except for variations of energetics in the presence of the thiolate ligand (Fig. 3b, steps 6-12; Fig. 4b, steps 6-11). In the latter mechanism, however, the second CO molecule can be reduced to a CH<sub>2</sub> species by a sequence of proton/electron transfer steps (Fig. 4c, steps 14-17), strongly resembling the reduction of the first CO molecule. The resulting, highly reactive CH<sub>2</sub> moiety can then be combined with the

CH<sub>3</sub> moiety at the proximal Fe atom to form an Fe-bound ethyl species with an energy barrier of only ~7 kcal/mol (Fig. 4c, step 18). Exothermic proton or coupled proton/electron transfer and ethane formation close the cycle (Fig. 4c, steps 19a, 19b). Coordination of a second CO molecule to the ethyl-bound cluster is energetically feasible and could explain the formation of longer carbon chains following the same sequence of events that lead to the formation of the C<sub>2</sub> species (Fig. 4c, steps 13-18), although the chain extension process would occur at a significantly reduced efficiency due to the multitude of competing reactions.

Based on these calculations, a constantly high supply of electrons would steer the reactivity of the cluster from CO dissociation (Figs. 3a and 4a, steps 4, 5) towards CO reduction (Fig. 3b, steps 6-12; Fig. 4b, steps 6-11), which is corroborated by the experimentally observed increase of the hydrocarbon/CO ratio in response to increasing amounts of reductant (Fig. 1a). Moreover, consistent with the calculation-based proposal of an aldehyde-like intermediate, [Fe<sub>4</sub>S<sub>4</sub>]<sup>Syn</sup> was shown to reduce formaldehyde (CH<sub>2</sub>O) at a yield of 16 nmol CH<sub>4</sub>/nmol cluster (Fig. 5a), and GC-MS analysis further demonstrated the expected mass shift and fragmentation pattern of the product CH<sub>4</sub> upon substitution of <sup>13</sup>CH<sub>2</sub>O for <sup>12</sup>CH<sub>2</sub>O, thereby confirming that the carbon in CH<sub>4</sub> originated from CH<sub>2</sub>O (Fig. 5b-e). Of the CO reduction events, however, C-C coupling has to compete with protonation of the CH<sub>3</sub> moiety, which can occur for every intermediate and which would consequently generate intermediates for CH<sub>4</sub> formation (Figs. 3b, 4b), thereby further increasing the yield of CH<sub>4</sub>.

The ability of [Fe<sub>4</sub>S<sub>4</sub>] clusters to catalyse the ambient reduction of CO<sub>2</sub> and CO to hydrocarbons could have implications for the prebiotic evolution of organic molecules, as previous studies have suggested a role of Fe- or FeS-containing minerals around underseas hypothermal vents in forming

hydrocarbons and other organic molecules in the presence of CO<sub>2</sub><sup>21-24</sup>. It has been demonstrated that CO can react with CH<sub>3</sub>SH on coprecipitated FeS and NiS to form carboxylic acids, carbohydrates and amino acids<sup>25-28</sup>, suggesting a prebiotic CO fixation pathway that could be correlated to the emergence of primordial lipids, sugars and peptides/proteins on Earth (see Supplementary Discussion). By analogy, the reduction of CO by FeS clusters in a speculated, highly reducing early atmosphere might represent another prebiotic route of CO activation, which generates small alkenes and alkanes as carbon and/or electron sources for certain methane- and ethene-assimilating organisms<sup>29,30</sup>. It is plausible, therefore, that the activity of NifH $^{Ma}$  in reducing CO<sub>2</sub> to hydrocarbons may represent an evolutionary relic of the function of FeS proteins in methanogens. Given the CO<sub>2</sub>-rich habitats of many methanogenic organisms, the differential abilities of the methanogenic and non-methanogenic organisms to handle CO<sub>2</sub> may account for the differential reactivities of the [Fe<sub>4</sub>S<sub>4</sub>] clusters in NifH<sup>Av</sup> and NifH<sup>Ma</sup> toward CO<sub>2</sub>. While the impact of protein environments on the reactivities of these biogenic [Fe<sub>4</sub>S<sub>4</sub>] clusters awaits further investigation, the reaction pathway proposed for the [Fe<sub>4</sub>S<sub>4</sub>] cluster serves as a good starting point for further exploration of the mechanism of FeS-based ambient reduction of CO2, which will in turn facilitate future development of FeS catalysts that convert the greenhouse gas CO2 into useful fuel products.

#### Methods

**Materials.** Unless otherwise specified, all chemicals were purchased from Thermo-Fisher Scientific (Waltham, MA) and Sigma-Aldrich (St. Louis, MO). Natural abundance <sup>12</sup>CO (99.9% purity) and <sup>12</sup>CO<sub>2</sub> (99.98% purity) were purchased from Praxair (Danbury, CT). Isotopologues <sup>13</sup>CO (99% isotopic purity) and <sup>13</sup>CO<sub>2</sub> (99% isotopic purity) were purchased from Cambridge Isotope Laboratories (Andover, MA). An Fe/S/Mo/V standard solution for metal content determination was purchased from Inorganic Ventures (Christiansburg, VA). Air-free manipulations were performed in a Vacuum Atmospheres (Hawthorne, CA) Omni-lab glovebox with an argon atmosphere operating at <2 ppm O<sub>2</sub>. Water was purified using a

Barnstead E-Pure water purification system (Thermo Scientific). Organic solvents were dried over columns containing Q-5 and molecular sieves and sparged with Ar; the solvents were stored over molecular sieves in the glovebox. Triethylammonium tetrafluoroborate ([Et<sub>3</sub>NH(BF<sub>4</sub>)]), samarium(II) diiodide tetrahydrofuran adduct ([SmI<sub>2</sub>(THF)<sub>2</sub>]), and the [Fe<sub>4</sub>S<sub>4</sub>]<sup>Syn</sup> cluster ([Ph<sub>4</sub>P]<sub>2</sub>[Fe<sub>4</sub>S<sub>4</sub>(SCH<sub>2</sub>CH<sub>2</sub>OH)<sub>4</sub>]) were prepared as described earlier<sup>18,31,32</sup>.

Cell growth and protein purification. An Azotobacter vinelandii strain expressing a non-tagged, nifH-encoded Fe protein of the Mo-nitrogenase (designated NifH<sup>Av</sup>) was grown as described elsewhere<sup>33,34</sup>. An Escherichia coli strain expressing a His-tagged, nifH-encoded Fe protein of the Mo-nitrogenase of Methanosarcina acetivorans (designated NifH<sup>Ma</sup>) was grown as reported earlier<sup>11</sup>. Published methods were used for the purification of NifH<sup>Av</sup> and NifH<sup>Ma</sup> from their respective expression strains<sup>11,33,34</sup>.

Redox potential determination. Redox titration was performed at ambient temperature in a glove box under anaerobic conditions. A series of NifH<sup>Ma</sup> samples were prepared in a 20 mM Tris–HCl buffer (pH 8.0) at a protein concentration of 2.5 mg/mL. Redox mediator dyes, including methyl viologen, benzyl viologen, safranin O and phenosafranin, were added at a final concentration of 10 μM to the series of NifH<sup>Ma</sup> protein samples. Subsequently, these samples were first reduced by excess sodium dithionite (DT; Na<sub>2</sub>S<sub>2</sub>O<sub>4</sub>) and then subjected to oxidative titration with 1 mM potassium ferricyanide. Reduction potentials were monitored with a combination electrode comprising a platinum working electrode and a saturated Ag/AgCl reference electrode (Microelectrodes, Inc., Bedford, NH), which were used to report potentials relative to the standard hydrogen potential (SHE). After achieving the desired potential, a 200 μL aliquot of each mixture was transferred to a capped quartz cuvette, and the transition between the [Fe<sub>4</sub>S<sub>4</sub>]<sup>1+/2+</sup> couple was monitored at 420 nm by UV/vis spectroscopy.

Assays of CO- and CO<sub>2</sub>-reduction with Fe proteins. The *in vitro* CO- and CO<sub>2</sub> reduction assays were carried out in 9.4 mL assay vials with crimped butyl rubber serum stoppers. Each assay contained, in a total volume of 1.0 mL, 500 mM Tris–HCl (pH 10.0, for CO<sub>2</sub> reduction assays) or 250 mM Tris–HCl (pH 8.0, for CO reduction assays), 0.5 mg Fe protein (NifH<sup>Av</sup> or NifH<sup>Ma</sup>), and either 200 mM dithionite or increasing concentrations (10, 20, 40 or 100 mM) of europium(II) diethylenetriaminepentaacetate (Eu<sup>II</sup>–DTPA). The optimum concentration of CO (0.53%) or CO<sub>2</sub> (100%) that yielded the maximum amount of product was determined via titration against increasing concentrations of CO or CO<sub>2</sub> and added to the headspace of the respective assay for activity analysis. For reactions of CO reduction, assays were assembled by repeatedly flushing and exchanging the buffer solution (without Eu<sup>II</sup>–DTPA and protein) with 100% Ar, followed by the addition of 0.53% CO; whereas for reactions of CO<sub>2</sub> reduction, assays were assembled by repeatedly

flushing and exchanging the buffer solution (without  $Eu^{II}$ –DTPA and protein) with 100%  $CO_2$ , and equilibrating for 30 min until pH stabilized at approximately 8.1. The reaction was initiated by the addition of Fe protein, followed immediately by the addition of  $Eu^{II}$ –DTPA and incubation with continuous shaking at 30°C until the reaction was complete (300 min) before it was quenched by the addition of 100  $\mu$ L of 30% trichloroacetic acid. Subsequently, headspace samples were taken to examine the production of CO and hydrocarbons.

Assays of CO oxidation with Fe proteins. The *in vitro* CO oxidation assays were carried out under 100% CO in 9.4 mL assay vials with crimped butyl rubber serum stoppers. Each assay contained, in a total volume of 1.0 mL, 250 mM Tris–HCl (pH 8.0), 10 mg NifH<sup>Av</sup> or NifH<sup>Ma</sup>, and 20 mM IDS. All assays were assembled by repeatedly flushing and exchanging the buffer solution (without IDS and protein) first with 100% Ar and then with 100% CO, followed by equilibration for 30 min. The reaction was initiated by the addition of Fe protein, followed immediately by the addition of IDS and incubation with continuous shaking at 30°C until the reaction was complete (300 min). Subsequently, 100  $\mu$ L concentrated hydrochloric acid (HCl) was added to each assay to release the dissolved CO<sub>2</sub> before the headspace sample was examined for the production of CO<sub>2</sub>.

Assays of CO- and CO<sub>2</sub>-reduction with [Fe<sub>4</sub>S<sub>4</sub>]<sup>Syn</sup> clusters and SmI<sub>2</sub>. The SmI<sub>2</sub>(THF)<sub>2</sub> stock solution was prepared by dissolving solid SmI<sub>2</sub>(THF)<sub>2</sub> in dry THF. The reaction buffer was prepared by dissolving Et<sub>3</sub>NH(BF<sub>4</sub>) in dry dimethylformamide (DMF), followed by addition of 1.5% (v/v) triethylamine (Et<sub>3</sub>N). A stock solution of the [Fe<sub>4</sub>S<sub>4</sub>]<sup>Syn</sup> cluster ([Ph<sub>4</sub>P]<sub>2</sub>[Fe<sub>4</sub>S<sub>4</sub>(SCH<sub>2</sub>CH<sub>2</sub>OH)<sub>4</sub>]) was prepared by dissolving crystals of the cluster in dry DMF. Assays were performed in 9.4 mL assay vials with crimped butyl rubber serum stoppers. Each assay contained, in a total volume of 1 mL, 100 mM Et<sub>3</sub>NH(BF<sub>4</sub>), 2 µM [Fe<sub>4</sub>S<sub>4</sub>]<sup>Syn</sup>, and 20 mM SmI<sub>2</sub>(THF<sub>2</sub>). In addition, the headspace of each assay contained 100% CO or CO<sub>2</sub>, which was determined as the optimum concentration that yielded the maximum amount of products via titration against increasing concentrations of CO or CO<sub>2</sub>. The negative controls had the same composition as the assays, except for the omission of either the cluster or the substrate. The reaction was initiated with the addition of [Fe<sub>4</sub>S<sub>4</sub>]<sup>Syn</sup>, followed immediately by injection of SmI<sub>2</sub> via a syringe. All assays and controls were incubated in a 30°C water bath shaker until the reaction was complete (10 min) before the headspace samples were taken and examined for hydrocarbon formation. The CO-reduction controls with FeCl<sub>3</sub> and FeCl<sub>3</sub>/Na<sub>2</sub>S lacked [Fe<sub>4</sub>S<sub>4</sub>]<sup>Syn</sup> and instead contained FeCl<sub>3</sub> that contained equimolar Fe to that of [Fe<sub>4</sub>S<sub>4</sub>]<sup>Syn</sup> in the absence or presence of Na<sub>2</sub>S at a 1:1 molar ratio to FeCl<sub>3</sub>. The reaction was initiated with the addition of FeCl<sub>3</sub> or FeCl<sub>3</sub>/Na<sub>2</sub>S, followed immediately by injection of SmI<sub>2</sub> via a syringe and incubation in a 30°C water bath

shaker until the reaction was complete (10 min) before the headspace samples were taken and examined for hydrocarbon formation.

Assays of CO- and CO<sub>2</sub>-reduction with [Fe<sub>4</sub>S<sub>4</sub>]<sup>Syn</sup> and Eu<sup>II</sup>–DTPA. The Eu<sup>II</sup>–DTPA stock solution was prepared by dissolving equimolar amounts of europium(II) chloride (EuCl<sub>2</sub>) and diethylenetriaminepenta-acetic acid (H<sub>5</sub>DTPA) to a final concentration of 200 mM in 1M Tris–HCl (pH 8.0) buffer. Assays were performed in 9.4 mL assay vials with crimped butyl rubber serum stoppers. Each assay for CO<sub>2</sub> reduction contained, in a total volume of 1 mL, 500 mM Tris–HCl (pH 9.8), 20 mM Eu<sup>II</sup>–DTPA, and 5 μM [Fe<sub>4</sub>S<sub>4</sub>]<sup>Syn</sup>, with 100% CO<sub>2</sub> in the headspace. This solution was allowed to sparge under CO<sub>2</sub> for 30 min until it reached saturation, when the pH of the solution stabilized at 7.8. Each reaction for CO reduction contained, in a total volume of 1 mL, 50 mM Tris–HCl (pH 7.8), 20 mM Eu<sup>II</sup>–DTPA, and 5 μM [Fe<sub>4</sub>S<sub>4</sub>]<sup>Syn</sup>, with 100% CO in the headspace atmosphere. The negative controls had the same composition as the assays, except for the omission of either the cluster or the substrate. The reaction was initiated by the addition of [Fe<sub>4</sub>S<sub>4</sub>]<sup>Syn</sup>, followed immediately by injection of Eu<sup>II</sup>–DTPA via a syringe. All assays and controls were incubated in a 30°C water bath shaker until the reaction was complete (60 min) before the headspace samples were taken and examined for hydrocarbon formation.

Quantification of CO and CO<sub>2</sub>. The amount of CO or CO<sub>2</sub> generated in the *in vitro* assays was determined through headspace analysis using a Thermo Scientific Trace 1300 Gas Chromatography with flame-ionization detector (GC–FID), in which the detector was interfaced with a methanizer (Thermo Electron North America LLC). CO or CO<sub>2</sub> in the headspace sample was separated on a TG-BOND Msieve 5A column (30 m × 0.32 mm ID × 30  $\mu$ m film; Thermo Electron North America LLC), which was held at 45°C for 1 min before it was heated to 110°C at a rate of 25°C/min. Subsequently, CO or CO<sub>2</sub> was hydrogenated at 350°C by the methanizer, and the resulting CH<sub>4</sub> was measured by GC–FID. The amount of CO or CO<sub>2</sub> was determined based on a linear standard curve ( $R^2 \ge 99.5$ ) that was derived from the measurement of varying amounts of CO or CO<sub>2</sub> using the same instrument. The detection limit for CO or CO<sub>2</sub> was 2 ppm.

Quantification of hydrocarbons. The hydrocarbon products CH<sub>4</sub>, C<sub>2</sub>H<sub>4</sub>, C<sub>2</sub>H<sub>6</sub>, C<sub>3</sub>H<sub>6</sub>, C<sub>3</sub>H<sub>8</sub>, 1-C<sub>4</sub>H<sub>8</sub>, *n*-C<sub>4</sub>H<sub>10</sub>, 1-C<sub>5</sub>H<sub>10</sub> and *n*-C<sub>5</sub>H<sub>12</sub> were measured on an activated alumina column (Grace, Deerfield, IL) in an SRI 8610C GC (SRI Instruments, Torrance, CA) equipped with a flame ionization detector (FID). From each headspace sample, a total of 250 μL gas was injected into the GC. The heating program for separating the gaseous products in the Eu<sup>II</sup>–DTPA-driven, aqueous assays was as follows: held at 55°C for 1 min; heated to 180°C at a rate of 12.5°C/min; and then held at 180°C for 0.6 min. The heating program for

separating the gaseous products in the  $SmI_2$ -driven, DMF-based assays was as follows: held at 55°C for 1 min; heated to 200°C at 12.5°C/min; and then held at 200°C for 3.6 min. The quantities of all products were determined as described previously<sup>35,36</sup> using a purchased gas mixture containing ~15 ppm of each hydrocarbon compound (Praxair, Geismar, LA).

Gas chromatography–mass spectrometry (GC–MS) analysis. Isotopic CO- and CO₂-reduction assays were prepared in the presence of <sup>12</sup>CO/<sup>13</sup>CO and <sup>12</sup>CO₂/<sup>13</sup>CO₂, respectively, for GC–MS analysis. The reaction products were then analysed by GC-MS using a Thermo Scientific Trace 1300 GC system coupled to a Thermo ISQ QD (Thermo Electron North America LLC) by comparing its mass and retention time with those of the <sup>12</sup>CO or <sup>13</sup>CO standard (≥99.9% purity), C₁-C₅ alkane hydrocarbon standard (containing 15 ppm of each gas), or a C₁-C₅ alkene hydrocarbon standard (containing 15 ppm of each gas). For each sample or standard, a total of 250 μL gas was injected into a split/splitless injector operated at 150°C in split mode with a split ratio of 10. Gas separation was achieved on a HP-PLOT/Q+PT column (30 m × 0.32 mm ID × 20 μm film; Agilent Technologies North America LLC), which was held at 30°C for 3 min, heated to 200°C at a rate of 15°C/min, and held at 200°C for 5 min. The rate at which the carrier gas, helium (He) passed through the column was held at 0.7 mL/min for 4 min, increased to 1.4 mL/min at a rate of 0.5 mL/min, and held at 1.4 mL/min for the duration of the run. The mass spectrometer was operated in electron impact (EI) ionization mode. The fragmentation patterns of the products were compared to standards and are consistent with those deposited in the NIST database (http://webbook.nist.gov).

**Density functional theory calculations.** Density functional theory (DFT) calculations of the mechanism of CO<sub>2</sub> reduction were carried out with the DFT programs in the Turbomole package, version 7.0<sup>37</sup>. Atomistic models of [Fe<sub>4</sub>S<sub>4</sub>](SCH<sub>2</sub>CH<sub>2</sub>OH)<sub>4</sub> ([Fe<sub>4</sub>S<sub>4</sub>]<sup>Syn</sup>) (see Lewis model in Supplementary Fig. 7a) and its carbon species-bound intermediates were built with Molden<sup>38</sup> and all atoms were allowed to relax fully during structure optimisations. Solvent effects were calculated implicitly by the conductor-like solvent screening model COSMO<sup>39</sup> as implemented in Turbomole, with a dielectric constant of  $\varepsilon$  = 37 and a solvent radius of 2.65 Å to represent the solvent DMF. The models were treated as open-shell systems in the unrestricted Kohn-Sham framework. Structural optimisations were performed with the TPSS functional<sup>40</sup> and a def2-TZVP<sup>41,42</sup> basis set assigned to all model atoms. Computational time was reduced by utilizing the resolution-of-the-identity approximation<sup>43,44</sup>. Antiferromagnetic coupling in the FeS cluster was accounted for by the broken symmetry approach<sup>45-47</sup>. All intermediates were optimised for at least three different spin states (S = 1/2, 3/2, 5/2 for systems with an odd number of electrons, and S = 0, 1, (2), 4 for those with an even number) in order to obtain low-energy solutions. All protonation energies were obtained

by considering the optimised cluster structure (TPSS, def2-TZVP, COSMO  $\varepsilon$ =37) and explicitly calculating the deprotonation energy of Et<sub>3</sub>NH<sup>+</sup>—the proton donor used in the DMF-based, cluster-catalysed reactions—in DMF (see Supplementary Fig.7b). The energies of all coordinating and dissociating species, including HSCH<sub>2</sub>CH<sub>2</sub>OH (Fig. 3, step 6), were calculated with the same settings. The energy of HSCH<sub>2</sub>CH<sub>2</sub>OH was also used to calculate the energy for re-ligating the cluster, where HSCH<sub>2</sub>CH<sub>2</sub>OH simultaneously acted as a proton donor (Fig. 3, steps 20a, 20b). Reduction energies were first calculated by assuming transfer of a free electron with zero kinetic energy. In order to obtain approximate redox free energies that better describe the energetics of the system, the resulting energies were then corrected with the reported experimental electrode potential of SmI<sub>2</sub>,  $E^{0}$ , = -1.5 V vs. SHE, following a previously described procedure<sup>48,49</sup>. This value was adapted to the DMF solvent with a previously reported value<sup>50</sup> for the relative electrode potential,  $\Delta E$  (SHE) = -4.34 V. The initially obtained reduction energies were transformed into redox free energies by adding the redox free energy of the reductant half reaction:  $\Delta G^0$  = -n F ( $E^0$ , -  $\Delta E$  (SHE)) (n, the number of electrons; F, Faraday constant)<sup>48,49</sup>. For SmI<sub>2</sub>, this value is -65.5 kcal/mol.

**Data availability.** The data that support the plots within this paper and other findings of this study are available from the corresponding author upon reasonable request.

#### **References:**

- 1. Burgess, B.K. & Lowe, D.J. Mechanism of molybdenum nitrogenase. *Chem. Rev.* **96**, 2983–3012 (1996).
- 2. Schilter, D., Camara, J.M., Huynh, M.T., Hammes-Schiffer, S. & Rauchfuss, T.B. Hydrogenase enzymes and their synthetic models: The role of metal hydrides. *Chem. Rev.* **116**, 8693–8749 (2016).
- 3. Mühlenhoff, U. et al. Compartmentalization of iron between mitochondria and the cytosol and its regulation. *Eur. J. Cell Biol.* **94**, 292–308 (2015).
- 4. O'Brien, E. et al. The [4Fe4S] cluster of human DNA primase functions as a redox switch using DNA charge transport. *Science* **355**, 813 (2017).
- 5. Mettert, E.L. & Kiley, P.J. Fe-S proteins that regulate gene expression. *Biochim. Biophys. Acta.* **1853**, 1284–1293 (2015).
- 6. Rees, D.C. et al. Structural basis of biological nitrogen fixation. *Philos. Trans. A Math. Phys. Eng. Sci.* **363**, 971–984 (2005).
- 7. Rees, D.C. & Howard, J.B. The interface between the biological and inorganic worlds: iron-sulfur metalloclusters. *Science* **300**, 929–931 (2003).

- 8. Georgiadis, M.M. et al. Crystallographic structure of the nitrogenase iron protein from *Azotobacter vinelandii*. *Science* **257**, 1653–1659 (1992).
- 9. Rebelein, J.G., Stiebritz, M.T., Lee, C.C. & Hu, Y. Activation and reduction of carbon dioxide by nitrogenase iron proteins. *Nat. Chem. Biol.* **13**, 147–149 (2017).
- 10. Rofer-DePoorter, C.K. A comprehensive mechanism for the Fischer-Tropsch synthesis. *Chem. Rev.* **81**, 447–474 (1981).
- 11. Hiller, C.J., Stiebritz, M.T., Lee, C.C., Liedtke, J. & Hu, Y. Tuning electron flux through nitrogenase with methanogen iron protein homologues. *Chemistry* **23**, 16152–16156 (2017).
- 12. Vincent, K.A. et al. Instantaneous, stoichiometric generation of powerfully reducing states of protein active sites using Eu(II) and polyaminocarboxylate ligands. *Chem. Commun.* **20**, 2590–2591 (2003).
- 13. Jeoung, J.H., Fesseler, J., Goetzl, S. & Dobbek, H. Carbon monoxide. Toxic gas and fuel for anaerobes and aerobes: carbon monoxide dehydrogenases. *Met. Ions. Life Sci.* **14**, 37–69 (2014)
- 14. Kung, Y. & Drennan, C.L. A role for nickel-iron cofactors in biological carbon monoxide and carbon dioxide utilization. *Curr. Opin. Chem. Biol.* **15**, 276–283 (2011).
- 15. Can, M., Armstrong, F.A. & Ragsdale, S.W. Structure, function, and mechanism of the nickel metalloenzymes, CO dehydrogenase, and acetyl-CoA synthase. *Chem. Rev.* **114**, 4149–4174 (2014).
- 16. Mayhew, S.G. The redox potential of dithionite and SO<sub>2</sub><sup>-</sup> from equilibrium reactions with flavodoxins, methyl viologen and hydrogen plus hydrogenase. *Eur. J. Biochem.* **85**, 535–547 (1978).
- 17. Averill, B.A., Herskovitz, T., Holm, R.H. & Ibers, J.A. Synthetic analogs of the active sites of iron-sulfur proteins. II. Synthesis and structure of the tetra(mercapto-μ<sub>3</sub>-sulfido-iron) clusters, (Fe<sub>4</sub>S<sub>4</sub>(SR)<sub>4</sub>)<sup>2</sup>-. J. Am. Chem. Soc. **95**, 3523–3534 (1973).
- 18. Barclay, J.E., Davies, S.C., Evans, D.J., Hughes, D.I. & Longhurst, S. Lattice effects in the Mössbauer spectra of salts of [Fe<sub>4</sub>S<sub>4</sub>{S(CH<sub>2</sub>)<sub>n</sub>OH}<sub>4</sub>]<sup>2-</sup>. Crystal structures of [PPh<sub>4</sub>]<sub>2</sub>[Fe<sub>4</sub>S<sub>4</sub>{S(CH<sub>2</sub>)<sub>n</sub>OH}<sub>4</sub>] (n=2, 3 and 4). *Inorg. Chim. Acta.* **291**, 101–108 (1999).
- 19. Sickerman, N.S., Hu, Y. & Ribbe, M.W. Activation of CO<sub>2</sub> by vanadium nitrogenase. *Chem. Asian. J.* **12**, 1985–1996 (2017).
- 20. Dance, I. How does vanadium nitrogenase reduce CO to hydrocarbons? *Dalton Trans.* **40**, 5516–5527 (2011).
- 21. Proskurowski, G. et al. Abiogenic hydrocarbon production at lost city hydrothermal field. *Science* **319**, 604–607 (2008).

- 22. McDermott, J.M., Seewald, J.S., German, C.R. & Sylva, S.P. Pathways for abiotic organic synthesis at submarine hydrothermal fields. *Proc. Natl. Acad. Sci. USA* **112**, 7668–7672 (2015).
- 23. Novikov, Y. & Copley, S.D. Reactivity landscape of pyruvate under simulated hydrothermal vent conditions. *Proc. Natl. Acad. Sci. USA* **110**, 13283–13288 (2013).
- 24. Roldan, A. et al. Bio-inspired CO<sub>2</sub> conversion by iron sulfide catalysts under sustainable conditions. *Chem. Commun. (Camb)* **51**, 7501–7504 (2015).
- 25. Huber, C. & Wächtershäuser, G. Activated acetic acid by carbon fixation on (Fe,Ni)S under primordial conditions. *Science* **276**, 245–247 (1997).
- 26. Scheidler, C., Sobotta, J., Eisenreich, W., Wächtershäuser, G. & Huber, C. Unsaturated C3,5,7,9-monocarboxylic acids by aqueous, one-pot carbon fixation: possible relevance for the origin of life. *Sci. Rep.* **6**, 27595 (2016).
- 27. Huber, C. & Wächtershäuser, G. Alpha-Hydroxy and alpha-amino acids under possible Hadean, volcanic origin-of-life conditions. *Science* **314**, 630–632 (2006).
- 28. Huber, C. & Wächtershäuser, G. Peptides by activation of amino acids with CO on (Ni,Fe)S surfaces: implications for the origin of life. *Science* **281**, 670–672 (1998).
- 29. Roslev, P., Iversen, N. & Henriksen, K. Oxidation and assimilation of atmospheric methane by soil methane oxidizers. *Appl. Environ Microbiol.* **63**, 874–880 (1997).
- 30. Coleman, N.V. & Spain, J.C. Distribution of the coenzyme M pathway of epoxide metabolism among ethene- and vinyl chloride-degrading Mycobacterium strains. *Appl. Environ. Microbiol.* **69**, 6041–6046 (2003).
- 31. Saba, S. et al. A simple and efficient one-step protocol for the preparation of alkyl-substituted ammonium tetrafluoroborate and hexafluorophosphate salts *J. Fluor. Chem.* **153**, 168–171 (2013).
- 32. Evans, W.J. et al. Solution synthesis and crystallographic characterization of the divalent organosamarium complexes (C<sub>5</sub>Me<sub>5</sub>)<sub>2</sub>Sm(THF)<sub>2</sub> and [(C<sub>5</sub>Me<sub>5</sub>)Sm(μ-I)(THF)<sub>2</sub>]<sub>2</sub>. J. Am. Chem. Soc. **107**, 941–946 (1985).
- 33. Lee, C.C., Hu, Y. & Ribbe, M.W. Stepwise formation of P-cluster in nitrogenase MoFe protein. *Proc. Natl. Acad. Sci. U. S. A.* **106**, 9209–9214 (2009).
- 34. Hu, Y., Fay, A.W. & Ribbe, M.W. Identification of a nitrogenase FeMo cofactor precursor on NifEN complex. *Proc. Natl. Acad. Sci. U. S. A.* **102**, 3236–3241 (2005).
- 35. Lee, C.C., Hu, Y. & Ribbe, M.W. Vanadium nitrogenase reduces CO. Science 329, 642 (2010).
- 36. Hu, Y., Lee, C.C. & Ribbe, M.W. Extending the carbon chain: hydrocarbon formation catalyzed by vanadium/molybdenum nitrogenases. *Science* **333**, 753–755 (2011).
- 37. Ahrichs, R., Bär, M., Häser, M., Horn, H. & Kömel, C. Electronic structure calculations on workstation computers: The program system Turbomole. *Chem. Phys. Lett.* **162**, 165–169 (1989).

- 38. Schaftenaar, G. & Noordik, J.H. Molden: a pre- and post-processing program for molecular and electronic structures. *J. Comput.-Aided Mol. Design* **14**, 123–134 (2000).
- 39. Klamt, A. & Schüürmann, G. COSMO: a new approach to dielectric screening in solvents with explicit expressions for the screening energy and its gradient. *J. Chem. Soc., Perkin Trans.* **2**, 799–805 (1993).
- 40. Tao, J., Perdew, J.P., Staroverov, V.N. & Scuseria, G.E. Climbing the density functional ladder: Nonempirical meta-generalized gradient approximation designed for molecules and solids. *Phys. Rev. Lett.* **91**, 146401 (2003).
- 41. Schäfer, A., Huber, C. & Ahlrichs, R. Fully optimized contracted Gaussian basis sets of triple zeta valence quality for atoms Li to Kr. *J. Chem. Phys.* **100**, 5829–5836 (1994).
- 42. Weigend, F. & Ahlrichs, R. Balanced basis sets of split valence, triple zeta valence and quadruple zeta valence quality for H to Rn: Design and assessment of accuracy. *Phys. Chem. Chem. Phys.* 7, 3297–3305 (2005).
- 43. Eichkorn, K, Weigend, F., Treutler, O. & Ahlrichs, R. Auxiliary basis sets for main row atoms and transition metals and their use to approximate Coulomb potentials. *Theor. Chem. Acc.* **97**, 119–124 (1997).
- 44. Weigend, F. Accurate Coulomb-fitting basis sets for H to Rn. *Phys. Chem. Chem. Phys.* **8**, 1057–1065 (2006).
- 45. Noodleman, J. Valence bond description of antiferromagnetic coupling in transition metal dimers. *J. Chem. Phys.* **74**, 5737–5743 (1981).
- 46. Noodleman, J., Post, D. & Baerends, E. Symmetry breaking and ionization from symmetry equivalent inner shells and lone pairs in Xα theory. *Chem. Phys.* **64**, 159–166 (1982).
- 47. Noodleman, J., Peng, C.Y., Case, D.A. & Mouesca, J.M. Orbital interactions, electron delocalization and spin coupling in iron-sulfur clusters. *Coord. Chem.* **144**, 199–244 (1995).
- 48. Noodleman, L., Han Du, W.G., Fee, J.A., Götz, A.W. & Walker, R.C. Linking chemical electron-proton transfer to proton pumping in cytochrome c oxidase: broken-symmetry DFT exploration of intermediates along the catalytic reaction pathway of the iron-copper dinuclear complex. *Inorg Chem.* 53, 6458–6472 (2014).
- 49. Torres, R.A., Lovell, T., Noodleman, L. & Case, D.A. Density functional and reduction potential calculations of Fe<sub>4</sub>S<sub>4</sub> clusters. *J. Am. Chem. Soc.* **125**, 1923–1936 (2003).
- 50. Tissandier, M.D. et al. The proton's absolute aqueous enthalpy and Gibbs free energy of solvation from cluster-ion solvation data. *J. Phys. Chem. A* **102**, 7787–7794 (1998).

**Acknowledgments:** We thank Prof. Markus Ribbe (UCI) for helpful discussions. This work was supported by NSF Career grant CHE-1651398 (to Y.H.), a grant-in-aid for Scientific Research (16H04116) from the Japanese Ministry of Education, Culture, Sports, Science and Technology (MEXT), Hori Sciences and Arts Foundation grant, and Takeda Science Foundation grant (to Y.O.).

#### **Author contributions**

Y.H. planned the research, M.T.S., C.J.H., N.S.S., C.C.L., K.T., and Y.O. performed the experiments, and Y.H. prepared the manuscript with suggestions of Y.O.

## **Competing interests**

The authors declare no competing interests.

#### **Additional information**

Supplementary information is available for this paper.

Correspondence and requests for materials should be addressed to Y.H.

#### **FIGURES**

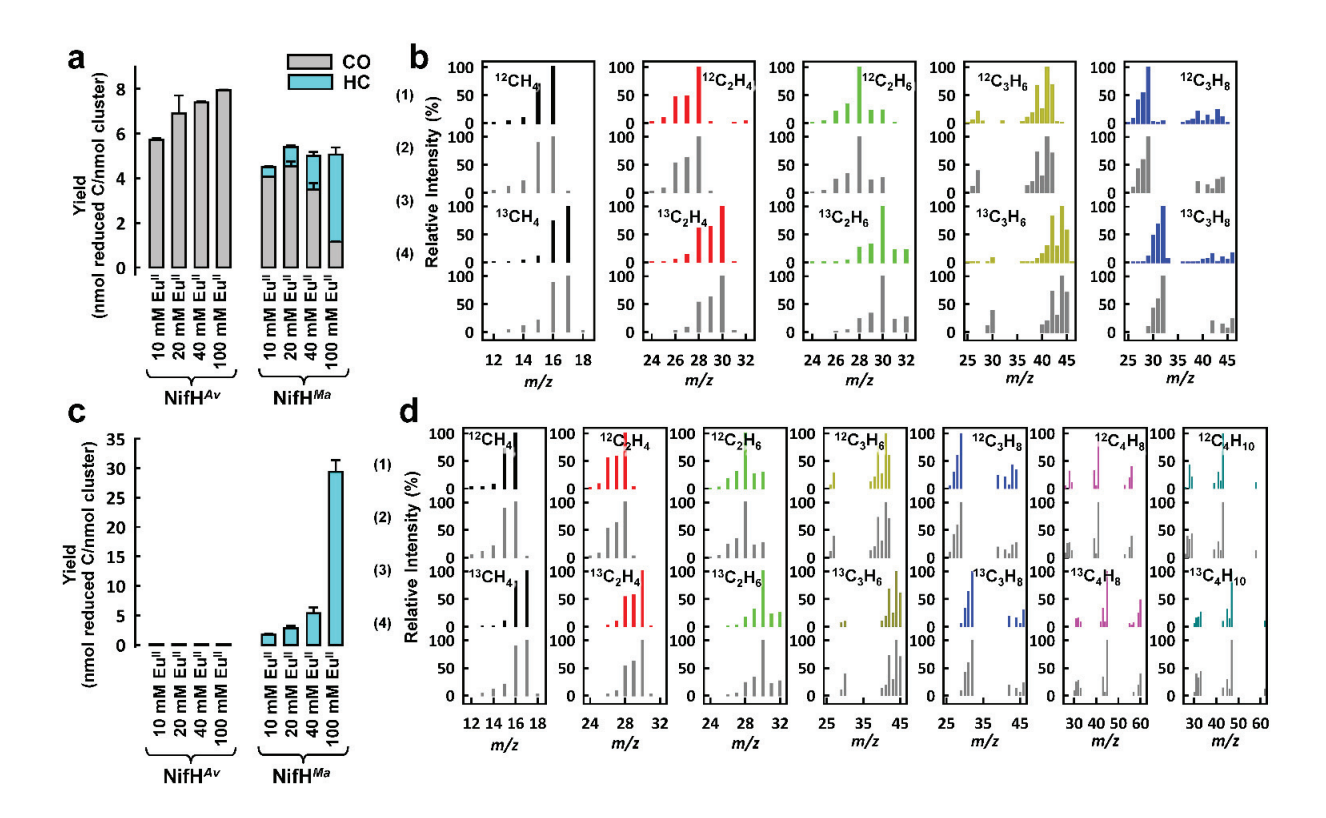


Fig. 1 | Reduction of CO<sub>2</sub> and CO by protein-bound [Fe<sub>4</sub>S<sub>4</sub>] clusters. (a, c) Yields of CO (grey) or hydrocarbons (cyan) generated from the reduction of CO<sub>2</sub> (a) or CO (c) by NifH<sup>Av</sup> or NifH<sup>Ma</sup> at increasing Eu<sup>II</sup>–DTPA concentrations. Yields were calculated based on nmol reduced C in CO or hydrocarbons per nmol cluster. HC, hydrocarbons; Eu<sup>II</sup>, Eu<sup>II</sup>–DTPA (b, d) GC-MS analysis of the hydrocarbon products generated from the reduction of <sup>12</sup>CO<sub>2</sub> (b, 1), <sup>13</sup>CO<sub>2</sub> (b, 3), <sup>12</sup>CO (d, 1) or <sup>13</sup>CO (d, 3) by NifH<sup>Ma</sup>, shown in comparison with the fragmentation patterns of the corresponding <sup>12</sup>C (b, d, 2) or <sup>13</sup>C (b, d, 4) labelled hydrocarbon standards. Colour code for GC-MS experimental data (1, 3): CH<sub>4</sub>, black; C<sub>2</sub>H<sub>4</sub>, red; C<sub>2</sub>H<sub>6</sub>, green; C<sub>3</sub>H<sub>6</sub>, yellow; C<sub>3</sub>H<sub>8</sub>, blue; C<sub>4</sub>H<sub>8</sub>, pink; C<sub>4</sub>H<sub>10</sub>, dark green. The corresponding hydrocarbon standards (2, 4) are shown in grey. Experiments that determined the product yields were performed three times (n=6), and data from these experiments are presented as mean±s.d.

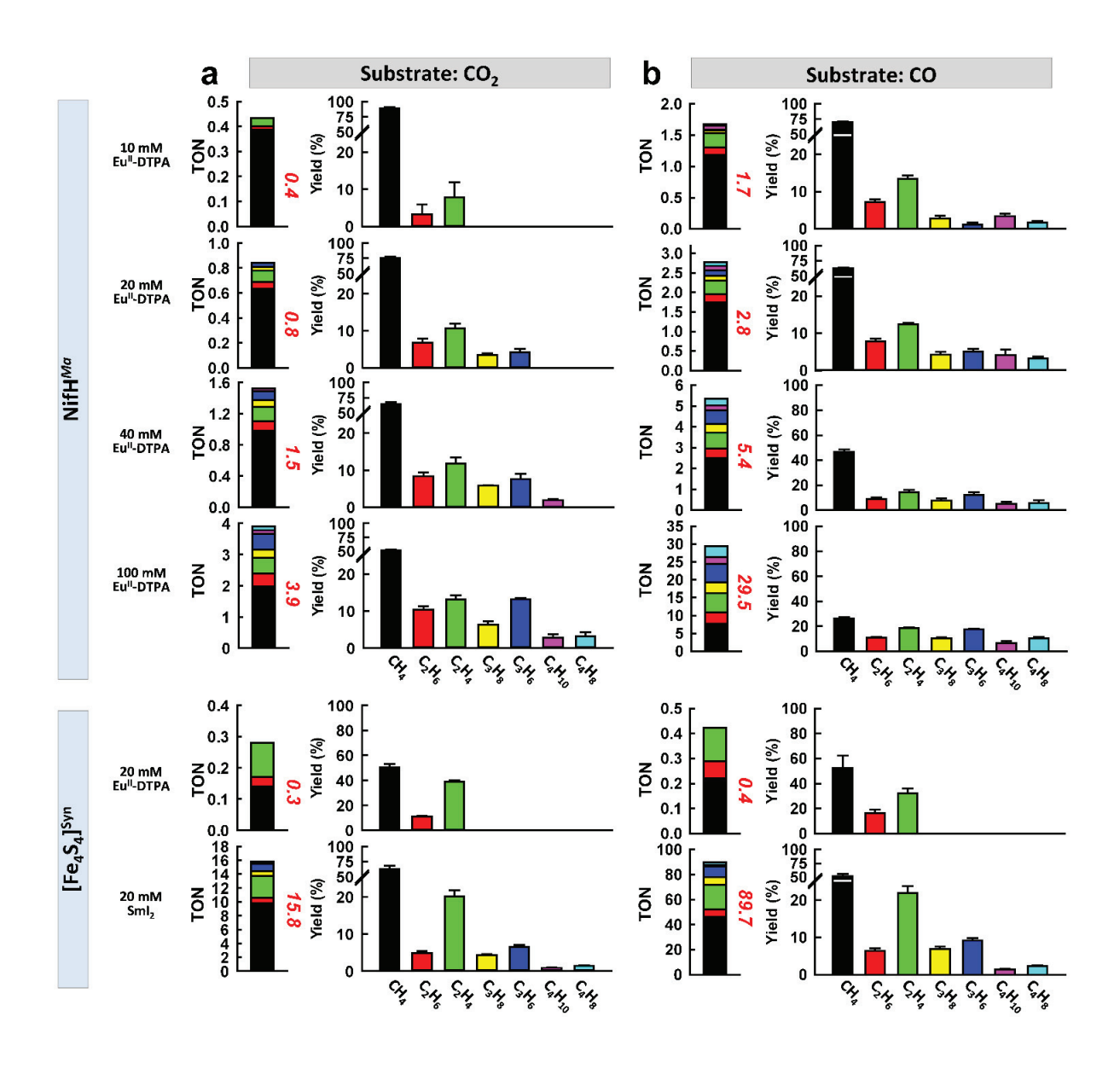


Fig. 2 | Formation of hydrocarbons by protein-bound and synthetic [Fe<sub>4</sub>S<sub>4</sub>] clusters. Turnover numbers (TONs) calculated based on all hydrocarbons (left charts) and percentage yields of individual hydrocarbon products (right charts) generated from the reduction of CO<sub>2</sub> (a) or CO (b) by NifH<sup>Ma</sup> at increasing Eu<sup>II</sup>–DTPA concentrations, or by [Fe<sub>4</sub>S<sub>4</sub>]<sup>Syn</sup> in the presence of Eu<sup>II</sup>–DTPA or SmI<sub>2</sub>. TONs, or total nmol reduced C in all hydrocarbons per nmol cluster, are shown in red fonts next to the stacked bars (a, b, left charts). Experiments that determined the product yields were performed three times (n=6), and data from these experiments are presented as mean±s.d.

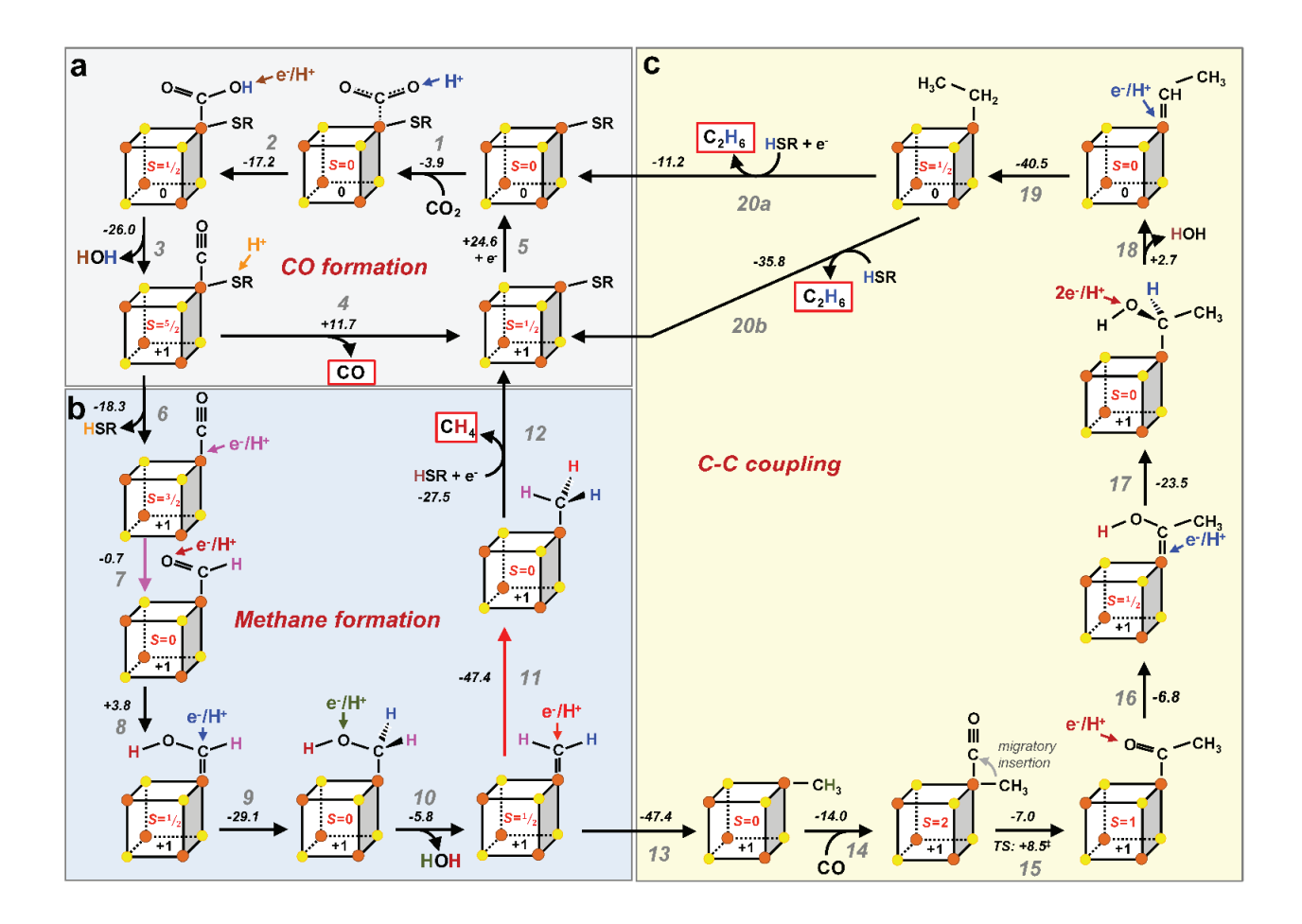


Fig. 3 | Proposed reaction pathway of CO<sub>2</sub> reduction catalysed by the [Fe<sub>4</sub>S<sub>4</sub>] cluster. Shown is the energetically plausible pathway derived from DFT calculations. Cluster ligand (-SR, SC<sub>2</sub>H<sub>4</sub>OH<sup>-</sup> or HSR, HSC<sub>2</sub>H<sub>4</sub>OH) is indicated as needed for the purpose of simplicity. The calculated reaction energy (kcal/mol) is indicated for each step (above or next to the arrow). (a) Coordination of CO<sub>2</sub> to a [Fe<sub>4</sub>S<sub>4</sub>]<sup>0</sup> cluster and release of CO upon reduction of CO<sub>2</sub>. (b) Reduction of a [Fe<sub>4</sub>S<sub>4</sub>]<sup>+</sup>-cluster-bound CO moiety to CH<sub>4</sub> via the formation of an aldehyde-like intermediate. (c) Formation of a C-C bond via migratory insertion that involves a [Fe<sub>4</sub>S<sub>4</sub>]<sup>+</sup>-cluster-bound -CH<sub>3</sub> species and a second CO molecule coordinated to the same Fe atom. See Supplementary Fig. 8a and 9a for the transition state and energy landscape of the proposed mechanism. TS, transition state.

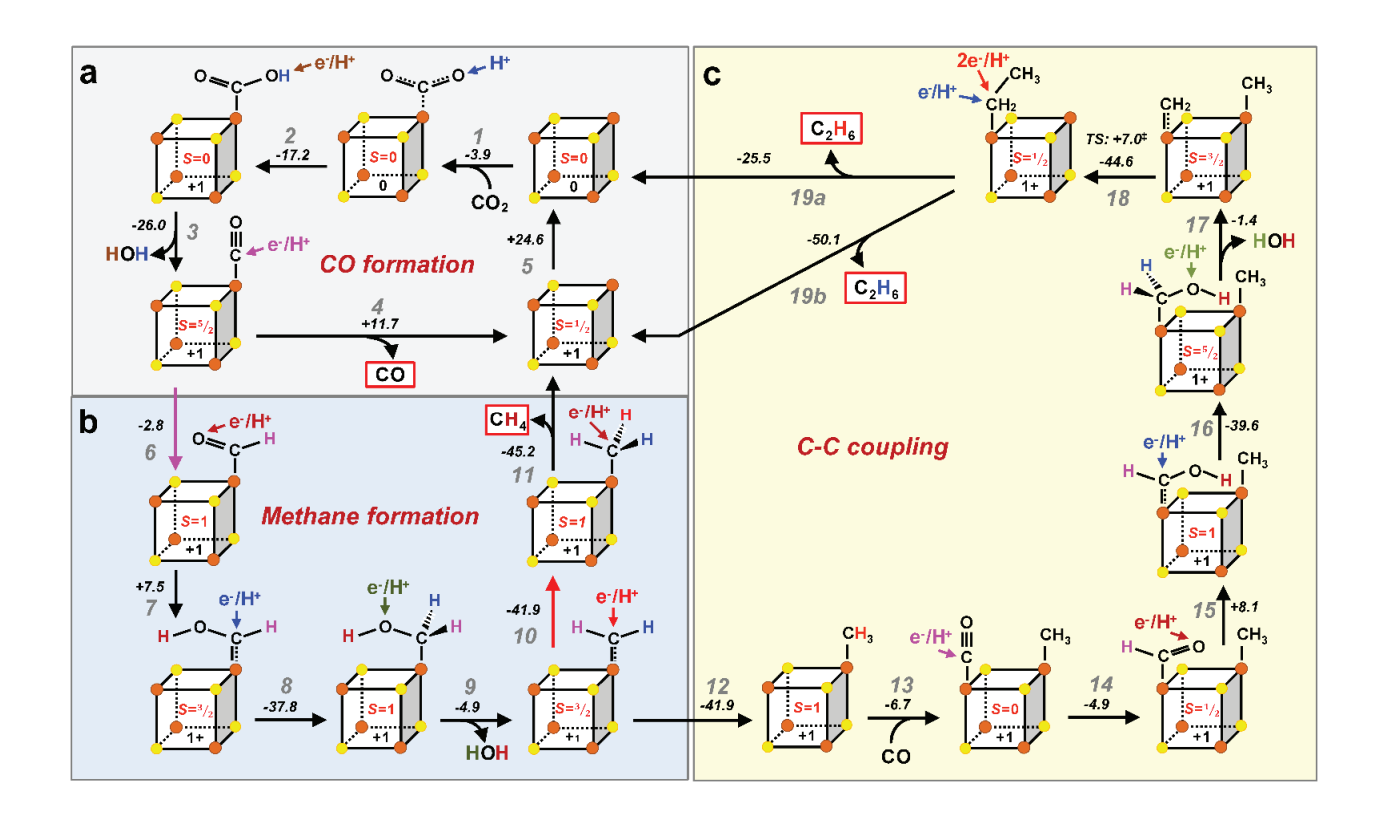


Fig. 4 | Alternative reaction pathway of CO<sub>2</sub> reduction catalysed by the [Fe<sub>4</sub>S<sub>4</sub>] cluster. Shown is the energetically plausible pathway derived from DFT calculations. The calculated reaction energy (kcal/mol) is indicated for each step (above or next to the arrow). Unlike the mechanism proposed in Fig. 3, this pathway doesn't involve dissociation of a thiolate ligand and proceeds by coordination events at two neighbouring Fe centres. Note that the thiolate groups are not depicted in the figure for the purpose of simplicity. (a) Coordination of CO<sub>2</sub> to a [Fe<sub>4</sub>S<sub>4</sub>]<sup>6</sup> cluster and release of CO upon reduction of CO<sub>2</sub>. (b) Reduction of a [Fe<sub>4</sub>S<sub>4</sub>]<sup>+</sup>-cluster-bound CO moiety to CH<sub>4</sub> via the formation of an aldehyde-like intermediate. (c) Formation of a C-C bond via coupling between a [Fe<sub>4</sub>S<sub>4</sub>]<sup>+</sup>-cluster-bound -CH<sub>3</sub> species with a reactive, bridged Fe-CH<sub>2</sub> intermediate that is derived from the second bound CO. See Supplementary Figs. 8b and 9b for the transition state and energy landscape of the proposed mechanism. TS, transition state. Other than the two plausible mechanisms presented in Figs. 3 and 4, reaction pathways involving protonation of the cluster sulphur atoms were also considered (Supplementary Figs. 10-12). However, given the initial strong endothermic coordination of CO<sub>2</sub> and structural destabilization of the cluster upon sulphur protonation, we strongly favour the mechanisms presented in Figs. 3 and 4.

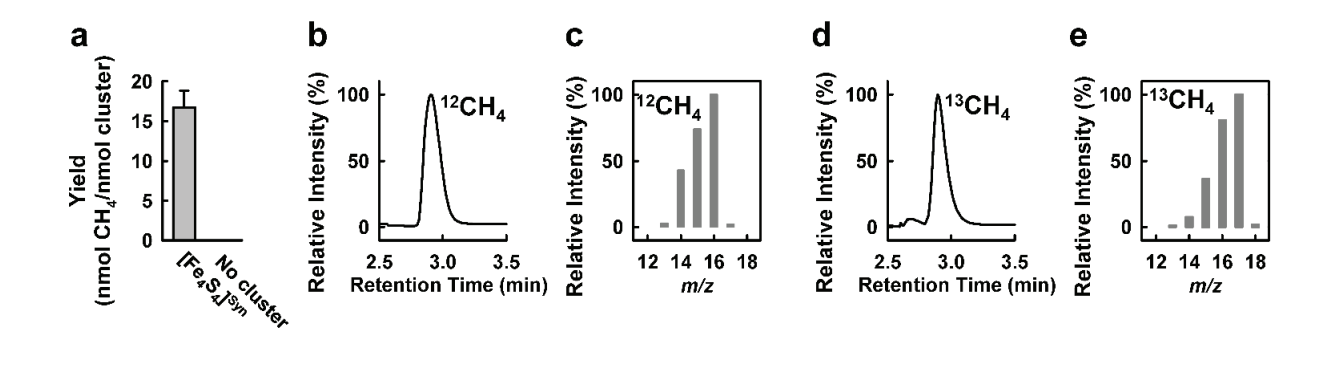


Fig. 5 | Reduction of CH<sub>2</sub>O to CH<sub>4</sub> by synthetic [Fe<sub>4</sub>S<sub>4</sub>] cluster. Turnover number (TON) calculated based on CH<sub>4</sub> generated from the reduction of CH<sub>2</sub>O (a), and GC-MS traces (b, d) and fragmentation patterns (c, e) of <sup>12</sup>CH<sub>4</sub> and <sup>13</sup>CH<sub>4</sub>, respectively, generated from the reduction of <sup>12</sup>CH<sub>2</sub>O (b, c) and <sup>13</sup>CH<sub>2</sub>O (d, e). The experiment that determined the product yield was performed three times (n=6), and data from this experiment is presented as mean±s.d.

## **Supplementary Information**

# Ambient Conversion of CO<sub>2</sub> to Hydrocarbons by Biogenic and Synthetic [Fe<sub>4</sub>S<sub>4</sub>] Clusters

Martin T. Stiebritz,<sup>1,a</sup> Caleb J. Hiller,<sup>1,2,a</sup> Nathaniel S. Sickerman,<sup>1,a</sup> Chi Chung Lee,<sup>1,a</sup> Kazuki Tanifuji,<sup>1</sup> Yasuhiro Ohki<sup>3</sup> & Yilin Hu<sup>1,\*</sup>

<sup>1</sup>Department of Molecular Biology and Biochemistry, University of California, Irvine, CA 92697-3900; <sup>2</sup>Department of Chemistry, University of California, Irvine, CA 92697-2025; <sup>3</sup>Department of Chemistry, Graduate School of Science, Nagoya University, Furo-cho, Chikusa-ku, Nagoya, 464-8602, Japan.

#### **Table of Contents**

## Supplementary Notes

Supplementary Note 1 Supplementary Note 2 Supplementary Note 3

## Supplementary Discussion

Fe protein (Fe<sub>4</sub>S<sub>4</sub>) *vs.* nitrogenase (cofactor) Fe<sub>4</sub>S<sub>4</sub> cluster *vs.* other Fe/S-based catalysts Fe<sub>4</sub>S<sub>4</sub> cluster *vs.* non-Fe/S catalysts

### Supplementary Figures

Supplementary Figure 1 Supplementary Figure 2 Supplementary Figure 3 Supplementary Figure 4 Supplementary Figure 5 Supplementary Figure 6 Supplementary Figure 7 Supplementary Figure 8 Supplementary Figure 9 Supplementary Figure 10 Supplementary Figure 11 Supplementary Figure 12

Supplementary References

#### **Supplementary Notes**

Supplementary Note 1: Transition states for the steps of C-C bond formation. For the rate-determining steps of the mechanisms depicted in Figs. 3 and 4, possible transition states were identified by optimizing distance-constrained structures along the expected reaction coordinates (C-C bond formation), followed by calculating the Hessian using the NumForce script provided with the Turbomole package and visualizing the normal modes with Jmol. Promising guess structures were then optimised with the statpt script provided with Turbomole, employing an eigenvector-following approach. Both transition states reported herein (Supplementary Fig. 8) show exactly one imaginary frequency, and the associated normal modes are consistent with the expected reaction coordinates. The transition states were further verified by calculating the reaction paths leading to the formation of product and reactant.

Supplementary Note 2: Other considered reaction pathways involving protonation of the cluster sulphur atoms. Protonation of the sulphur atoms of the all-ferrous [Fe<sub>4</sub>S<sub>4</sub>] cluster is exothermic by -14.3 kcal/mol. However, this protonation event disrupts and opens up the compact cubane structure by weakening the bond between the newly formed SH group and the proximal Fe atom (Supplementary Fig. 10), which provides an avenue for cluster destruction and contradicts our experimental findings of sustained catalytic turnover. Moreover, the x-ray crystallographic structure of the all-ferrous Fe protein further argues against disruption of its [Fe<sub>4</sub>S<sub>4</sub>] cluster, as the cluster remains intact in the all-ferrous state<sup>1</sup>. Nevertheless, we considered possible mechanistic routes starting from this unlikely cluster geometry for the sake of completeness (Supplementary Fig. 11).

Coordination of CO<sub>2</sub> to the protonated cluster is highly endothermic by +54.9 kcal/mol, (highlighted as a red box in Supplementary Fig. 11, step 2), and the subsequent reduction of its unlikely reaction product is exothermic by -37.0 kcal/mol (Supplementary Fig. 11, step 3). Taken together, these two initial steps of this reaction route would still be endothermic. However, we still considered plausible reaction events that occur subsequent to these initial steps. As can be seen from the scheme in Supplementary Fig. 11, reaction steps analogous to those proposed in Figs. 3 and 4 could in principle occur, which involve protonation of the CO<sub>2</sub> moiety, dissociation of an H<sub>2</sub>O molecule, and consecutive e<sup>-</sup>/H<sup>+</sup> transfers, yielding an Fe-bound CH<sub>3</sub>-species upon dissociation of an additional H<sub>2</sub>O molecule (Supplementary Fig. 11, step 11). In analogy to the mechanisms presented in Figs. 3 and 4, further electron/proton transfer steps result in exothermic methane formation (Supplementary Fig. 11, step 12). In two alternative scenarios, a second CO molecule can either coordinate to the Fe atom that is already bound with a CH<sub>3</sub> species (exothermic by -18.6 kcal/mol, Supplementary Fig. 11, step 14), thereby resembling the mechanism proposed in Fig. 3, or to the neighbouring Fe atom (exothermic by -4.3 kcal/mol, Supplementary Fig. 11, step 15), which corresponds to the scheme presented in Fig. 4. The first route, however, results in a dead-end; specifically, the migratory insertion step depicted in Fig. 3 cannot occur in the case of the open cluster, as structural optimisation of an activated complex leads to the re-formation of the end product of step 14. The second alternative, on the other hand, proceeds analogously to the mechanism depicted in Fig. 4, thereby corroborating the originally considered reaction steps.

In addition to the mechanism discussed in Supplementary Fig. 11, we considered the energetics of proton and coupled electron/proton transfer steps to various intermediates of the main mechanisms presented in Figs. 3 and 4. The results are shown in Supplementary Fig. 12, which

again indicate substantial cluster distortion and unfavourable energetics caused by protonation of the cluster sulphur atoms.

Taken together, given the initial strong endothermic coordination of CO<sub>2</sub> and structural destabilization of the cluster upon sulphur protonation, we strongly favour the mechanisms presented in Figs. 3 and 4 to those involving the protonation of cluster sulphur atoms.

**Supplementary Note 3: Coordination of CO<sub>2</sub> to the cluster.** As reported previously for the coordination of CO<sub>2</sub> to the [Fe<sub>4</sub>S<sub>4</sub>] cluster of the *A. vinelandii* Fe protein<sup>2</sup>, we only observed exothermic binding when CO<sub>2</sub> was directly coordinated to one of the Fe atoms of the all-ferrous [Fe<sub>4</sub>S<sub>4</sub>]<sup>0</sup> cluster in a singlet spin state (S=0). Alternative scenarios for different charge and spin states, or alternative binding sites, such as ligand and cluster S atoms, or sites exposed by opening of the cluster, resulted in strongly endothermic reaction energies. Previous EPR spectroscopic data suggest that the cluster can indeed adopt a S=0 spin state<sup>3</sup>. With the DFT approach described herein, the S=0 state of the ligand-free cluster is slightly less stable than the S=4 state (by ~4-5 kcal/mol). At ambient temperatures, the cluster might be represented best by a mixture of spin states. For all other forms that can be formally considered as existing in the all-ferrous state, the low-spin solution is more stable than the S=4 state [i.e., -2 to -3 kcal/mol for the CO<sub>2</sub>-bound form (see Figs. 3 and 4), -5 to -6 kcal/mol for the CO<sub>2</sub>H-bound form (see Figs. 3 and 4), and ~ -10 kcal/mol for the CHCH<sub>3</sub>-bound cluster (see Fig. 4, where the most favourable spin state is S=1)].

### **Supplementary Discussion**

The ambient reduction of CO to hydrocarbons is highly interesting because of its industrial potential and its plausible relevance to prebiotic chemistry. Here, we compare the reactivities of biogenic and synthetic [Fe<sub>4</sub>S<sub>4</sub>] clusters toward CO with those of several other notable systems, such as (1) the nitrogenase-based catalysts, including the catalytic component of nitrogenases (e.g., MoFe and VFe proteins) and the nitrogenase cofactors (e.g., M- and V-clusters); (2) the Fe/S-based catalysts, including those generated by synthetic approaches (e.g., synthetic FeS clusters) and those associated with prebiotic chemistry (e.g., Fe/S precipitates); and (3) the non-Fe/S catalysts, including homogeneous molecular catalysts (i.e., synthetic compounds) and heterogeneous surface catalysts (e.g., the Fischer-Tropsch catalysts).

## Fe protein (Fe<sub>4</sub>S<sub>4</sub>) vs. nitrogenase (cofactor)

Fe protein vs. nitrogenase. The V-nitrogenase is the most active enzyme known to convert CO to hydrocarbons under ambient conditions<sup>4</sup>. Using its Fe protein component (VnfH<sup>Av</sup>) to deliver electrons to its catalytic VFe protein component (VnfDGK<sup>Av</sup>) in the presence of ATP and dithionite, the holo V-nitrogenase of A. vinelandii<sup>4,5</sup> averages approximately 14 turnovers of CO per minute in an in vitro assay and produces more than 50 times the yield of hydrocarbons relative to that produced by NifH<sup>Ma</sup>. In contrast, the holo Mo-nitrogenase of A. vinelandii reduces CO to hydrocarbons at a rate that is approximately 800-fold lower than that the V-nitrogenase when it utilizes its Fe protein component (NifH<sup>Av</sup>) to deliver electrons to its catalytic MoFe protein component (NifDK<sup>Av</sup>) in the presence of ATP and dithionite in an in vitro assay<sup>5</sup>. Under improved conditions, such as upon substitution of D<sub>2</sub>O for H<sub>2</sub>O in the assay<sup>5</sup>, the yield of hydrocarbon formation by Mo-nitrogenase is comparable to that by NifH<sup>Ma</sup>. In addition, certain variants of Monitrogenase have been reported to achieve 20-30 turnovers over the course of the reaction<sup>6</sup>, which is comparable to that of NifH<sup>Ma</sup>.

The higher activity of the holo nitrogenase than its Fe protein component in CO reduction is not surprising, given the intricate two-component mechanism employed by nitrogenase that renders it efficient in transferring electrons to the cofactor site, rendering the cofactor in a sufficiently low redox potential for substrate binding and reduction. Moreover, the high-nuclearity metallocofactors likely provide more reaction sites than the smaller [Fe<sub>4</sub>S<sub>4</sub>] clusters, which could further account for a higher activity of these clusters in catalysing CO reduction. The disadvantages of this system, however, are the complexity of the reaction mechanism and the ATP-dependent nature of the reaction, making it difficult to use this system for mechanistic investigations of CO reduction, as well as potential applications for industrial use in the future. In comparison, the Fe protein (i.e., NifH<sup>Ma</sup>) is a unique, stand-alone catalyst that can work in an ATP-independent manner, which makes it a simplified template for mechanistic investigations of FeS-based CO activation, as well as future development of strategies for ambient conversion of CO and CO<sub>2</sub> into useful chemical commodities.

*Fe<sub>4</sub>S<sub>4</sub> cluster vs. cofactor.* Other than the holo enzyme systems, simplified systems that are ATP-free and consist of only reductants and the cofactors isolated from the Mo- and V-nitrogenases (i.e., the M- and V- clusters) have been shown to reduce CO to hydrocarbons<sup>7-9</sup>. Both Eu<sup>II</sup>-DTPA and SmI<sub>2</sub> are effective in driving the reduction of CO to hydrocarbons by these systems. In the presence of Eu<sup>II</sup>-DTPA, the hydrocarbon yields of both M- and V- clusters are similar to that of [Fe<sub>4</sub>S<sub>4</sub>]<sup>Syn</sup> under the same reaction conditions<sup>7</sup>. In the presence of SmI<sub>2</sub>, the hydrocarbon yields of both M- and V-clusters are improved, and a recent study shows a TON of greater than 200 for the M-cluster<sup>10</sup>, which is approximately twice the TON of [Fe<sub>4</sub>S<sub>4</sub>]<sup>Syn</sup> reported in this work. The corresponding number for the V-cluster-catalysed CO reduction under the same reaction conditions has not been reported so far.

The higher activity of the isolated cofactor than the [Fe<sub>4</sub>S<sub>4</sub>] cluster in this reaction again illustrates the effectiveness of the complex, high-nuclearity metallocofactors in CO reduction, possibly due to the presence of more reaction sites on these larger clusters. However, the disadvantage of this system is the laborious process to isolate sufficient amounts of cofactors from the nitrogenase enzymes. In this light, the current report is unique in demonstrating the surprising ability of a much more accessible, synthetic [Fe<sub>4</sub>S<sub>4</sub>] cluster to drive difficult reactions of CO<sub>2</sub>- and CO-reduction at reasonable yields prior to any optimisation, suggesting this system as a potential candidate for future development of strategies of FeS-based conversion of CO and CO<sub>2</sub> to hydrocarbons under ambient conditions.

#### Fe<sub>4</sub>S<sub>4</sub> cluster vs. other Fe/S-based catalysts

Fe<sub>4</sub>S<sub>4</sub> cluster vs. synthetic FeS-based catalysts. While a large number of synthetic or biomimetic FeS-based clusters have been reported in the literature<sup>11-14</sup>, only a few of them have been described for their abilities to activate small molecules. These handful of examples include the sub-stoichiometric reduction of acetylene to ethylene by a synthetic [Fe<sub>4</sub>S<sub>4</sub>] cluster<sup>14</sup>, and the catalytic reduction of hydrazine to ammonia by [MoFe<sub>3</sub>S<sub>4</sub>] and [VFe<sub>3</sub>S<sub>4</sub>] clusters<sup>15,16</sup>. In addition, a report from 1992<sup>17</sup> describes the 2e<sup>-</sup>-reduction of CO<sub>2</sub> by a [Mo<sub>2</sub>Fe<sub>6</sub>S<sub>8</sub>(SEt)<sub>9</sub>]<sup>3-</sup> catalyst to a product which then reacts with a thioester (CH<sub>3</sub>COSEt in this case) to produce a β-ketoacid (RCOCOO<sup>-</sup>) and SEt<sup>-</sup>. The scarcity of early examples for CO<sub>2</sub>/CO reduction to hydrocarbons highlights the difficulty of these reactions to occur under ambient conditions. Recently, in light of the discovery of the reactivity of nitrogenase toward CO, two synthetic nitrogenase cofactor mimics—namely, a [Et<sub>4</sub>N]<sub>4</sub>[Fe<sub>6</sub>S<sub>9</sub>(SEt)<sub>2</sub>] cluster (synthesized by the Holm group)<sup>18</sup> and a [Cp\*MoFe<sub>5</sub>S<sub>9</sub>(SH)]<sup>3-</sup> cluster (synthesized by the Tatsumi group)<sup>10</sup>, which represent a

homometallic and a heterometallic analogue of the cofactor, respectively—were examined for their abilities to reduce CO and CO<sub>2</sub> to hydrocarbons. Interestingly, these two cofactor mimics demonstrated activities of hydrocarbon production from CO- and CO<sub>2</sub>-reduction that were comparable with, but lower than those of the nitrogenase cofactors under the same reaction conditions<sup>10,19</sup>. These results point to the possibility that more reports along this line will surface in the near future, which could help bridge the gap of our current knowledge on the reactivities of synthetic FeS-based catalytic systems toward CO<sub>2</sub> and CO.

Fe<sub>4</sub>S<sub>4</sub> cluster vs. Fe/S-containing precipitates. In their seminal work published in 1997, Huber and Wächtershäuser show that CO can react with CH<sub>3</sub>SH on coprecipitated NiS and FeS to form CH<sub>3</sub>COOH and H<sub>2</sub>S, with CH<sub>3</sub>-CO-SCH<sub>3</sub> being the potential intermediate of this reaction<sup>20</sup>. This result suggests a prebiotic CO fixation pathway that might be employed by the earliest organisms living around the hyperthermal vents underneath the deep oceans. Based on this work, a series of follow-up studies using CO as a carbon feedstock and/or an electron donor show that the product profile of this reaction can be substantially extended to include long chain carboxylic acids, carbohydrates (i.e., hydroxyl acids) and amino acids (when CN<sup>-</sup> or NH<sub>4</sub><sup>+</sup> is used as a co-reactant), with each of them correlated to the emergence of primordial lipids, sugars and peptides/proteins, respectively, on Earth<sup>21-24</sup>. By analogy, the reduction of CO by FeS clusters in a speculated, highly reducing early atmosphere might represent another prebiotic route of CO activation, which generates small alkenes and alkanes as carbon and/or electron sources for certain methane- and ethene-assimilating microorganisms<sup>25,26</sup> It has been postulated that in the Archean era, there was a methane- and CO-rich atmosphere and anoxic oceans inhabited by iron- and sulphur-metabolizing microbes, such as purple- and green-sulphur bacteria<sup>27</sup>. It is plausible that these microorganisms could produce small hydrocarbons via secondary metabolic pathways that parallel that reported in the case of A. vinelandii<sup>28</sup>, which were then assimilated by microorganisms utilizing hydrocarbons for cell growth.

There are some notable differences between these prebiotic synthesis systems and the [Fe<sub>4</sub>S<sub>4</sub>] cluster-based system reported in this work. One, the reaction described in our work is, in essence, a reductive coupling reaction of CO or CO<sub>2</sub> on the [Fe<sub>4</sub>S<sub>4</sub>] cluster (see mechanisms depicted in the main text); whereas the general reaction described in the pre-biotic synthesis models involves the capture of CO on a given carbon backbone through carbonylation, followed by further reaction of the carbonyl moiety to generate carboxylic acids or amino acids. Consequently, hydrocarbons have seldomly been reported as products generated by these models of pre-biotic synthesis. Two, the reaction reported in this work utilizes a homogeneous catalyst (i.e., the [Fe<sub>4</sub>S<sub>4</sub>] cluster); whereas the primordial model systems are essentially semi-heterogeneous, where substrates are activated on a slurry of material particles. Three, our reaction is driven by low reduction potentials delivered by strong reductants; whereas the prebiotic synthesis reactions are powered by high temperatures (above the boiling point) and often high pressures, and they are allowed to proceed over a much longer reaction timeframe<sup>20-23</sup>.

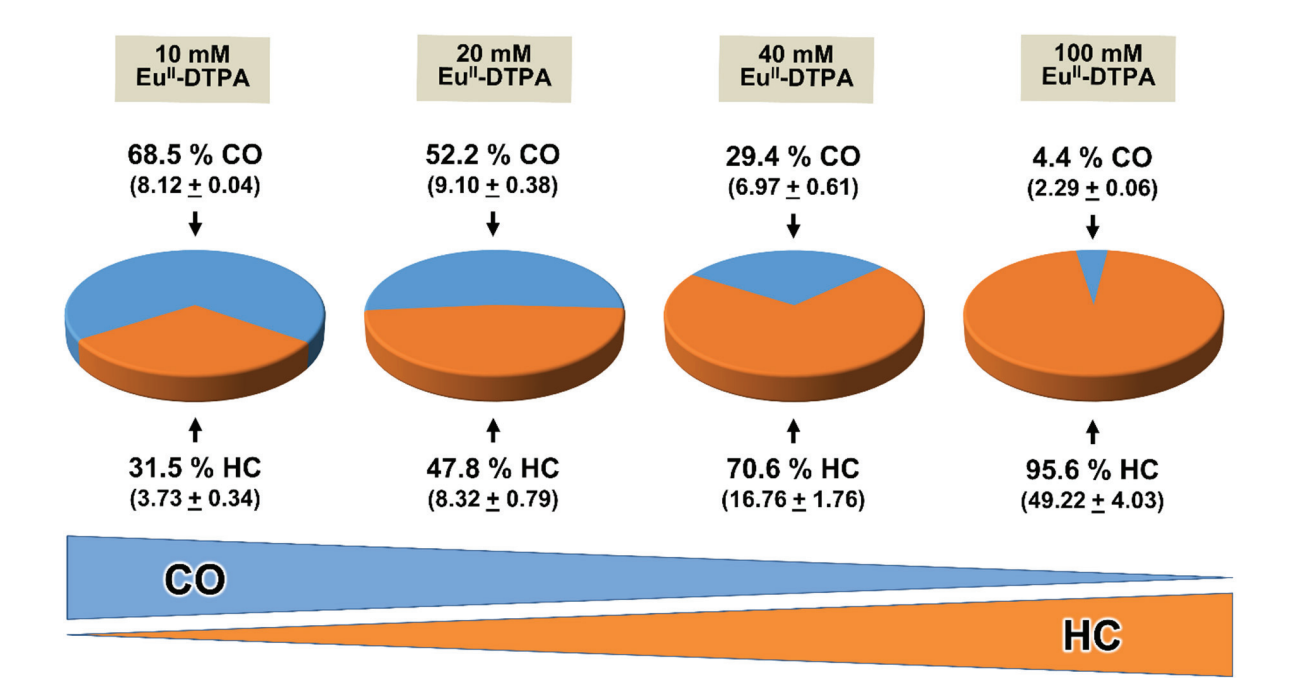
### Fe<sub>4</sub>S<sub>4</sub> cluster vs. non-Fe/S catalysts

 $Fe_4S_4$  cluster vs. homogeneous non-Fe/S catalysts. Several notable attempts have been made to convert the inactive carbon oxides to useful chemical compounds by combining these molecules with reactive or pre-activated organic compounds, such as the poly- and cyclic carbonate syntheses from  $CO_2^{29,30}$  and the Monsanto acetic acid synthesis from  $CO_3^{31}$ . In addition, synthetic compounds have been explored for their abilities to directly transform  $CO_2^{31}$  and  $CO_2^{31}$  into hydrocarbons. One such example was reported by Hou et al. in 2006, where tetranuclear lanthanide polyhydrido

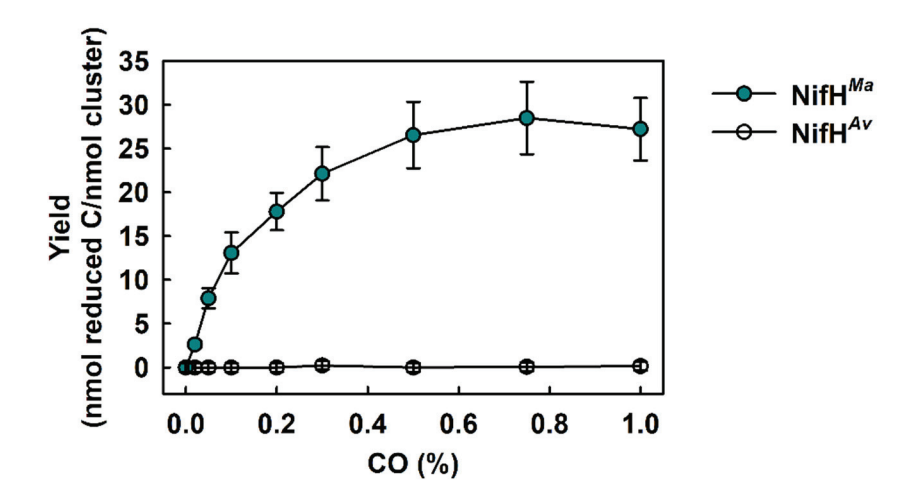
clusters were used for selective formation of  $C_2H_4$  from  $CO^{32}$ . This type of reaction is remarkable in that it achieves selective C-C coupling and cleavage of C-O bond at ambient temperature and pressure; however, the reactions are not catalytic because of the absence of a  $H^+$  source in these systems and, consequently, the need to remove O atoms from CO in the forms of  $Ln_4O_4$  and Si-O-Si species, resulting in the conversion of the catalysts into dead-end by-products, i.e.,  $Ln_4O_4$  clusters (Ln = Y or Lu).

Fe4S4 cluster vs. heterogeneous non-Fe/S catalysts. The best-known example of the heterogeneous catalysis of CO reduction is the Fischer-Tropsch (FT) process, which combines CO with H<sub>2</sub> into hydrocarbons. There are a number of points that distinguish the FT process<sup>33-35</sup> with the reaction reported in this work. One, our reaction occurs at ambient temperature and pressure; whereas the FT process, which is a gas-solid two-phase reaction, typically requires high temperature and pressure. Two, contrary to the reaction described in this report, the reactivity and product selectivity of the FT process vary greatly depending on the reaction conditions and the choice of catalysts. Three, the reaction catalysed by the [Fe<sub>4</sub>S<sub>4</sub>] cluster utilizes protons as the hydrogen source; whereas the reducing power of the FT process is provided in the form of molecular hydrogen. Other than the FT process, alternative strategies for the conversion of CO and CO<sub>2</sub> to hydrocarbons, such as the electrochemical reduction of these carbon oxides, have also been explored to circumvent the requirement of high temperature and pressure for the 2-phase catalysis. The products generated by these alternative approaches are mainly methane and ethene, and they typically require a metal surface, such as copper, for catalysis to occur<sup>36,37</sup>. While this electrode-based approach has the shortcomings in needing a relatively large overpotential for preferential hydrocarbon production and having a relatively low selectivity of products comparing to FT synthesis, it bears potential in supplying a continuous flow of electrons that may be combined with the [Fe<sub>4</sub>S<sub>4</sub>] cluster-based reaction to generate a continuous system for ambient conversion of CO and CO<sub>2</sub> to hydrocarbons.

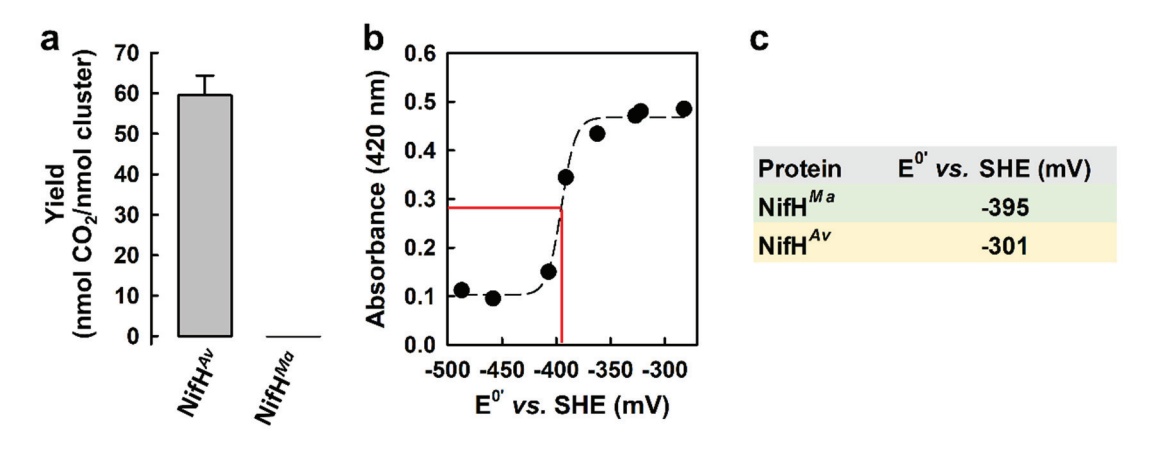
#### **Supplementary Figures**



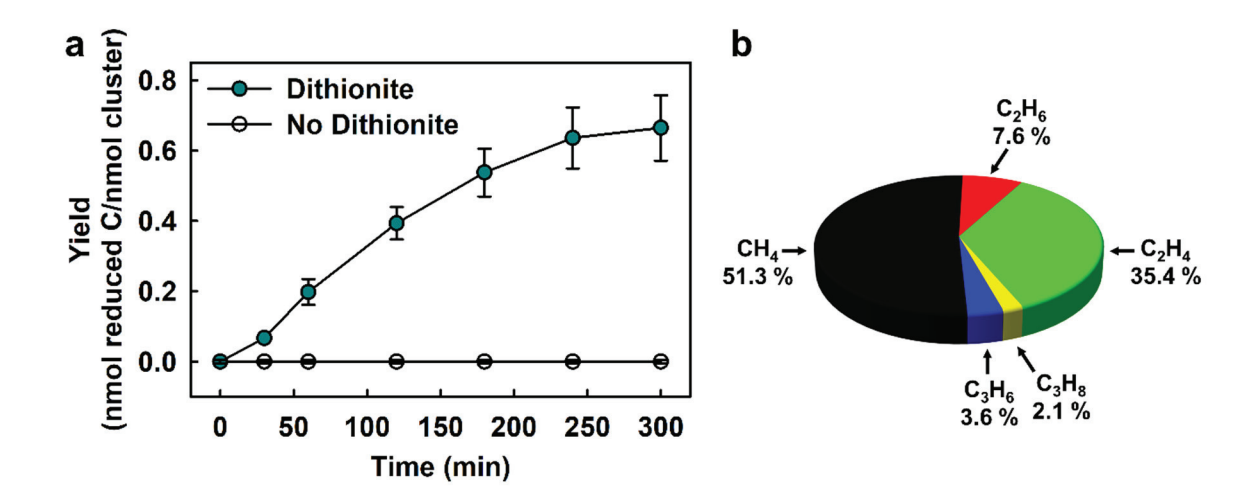
Supplementary Fig. 1 | Product distribution of CO<sub>2</sub> reduction in the presence of increasing amounts of reductant. Data are taken from Fig. 1a. The activity of CO or hydrocarbon (HC) formation from the reduction of CO<sub>2</sub> by NifH<sup>Ma</sup> is expressed as nmol electrons that appear in CO or HC per nmol cluster and shown in parentheses. The percentage distributions of electrons in CO and HC were calculated based on these numbers. The total amount of electrons that appear in products (both CO and HC) increases concomitantly with a shift toward HC formation when CO<sub>2</sub> is reduced by NifH<sup>Ma</sup> in the presence of increasing Eu<sup>II</sup>-DTPA concentrations. Experiments that determined the product yields (Fig. 1a) were performed three times (n=6), and data from these experiments are presented as mean±s.d.



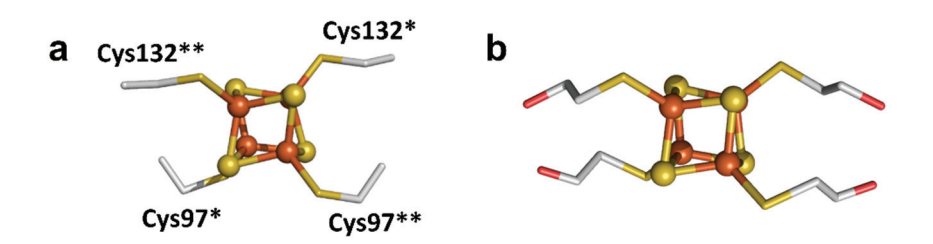
Supplementary Fig. 2 Titration of product yield versus CO concentration. Shown are the yields of hydrocarbons generated from increasing amounts of CO by NifH<sup>Av</sup> or NifH<sup>Ma</sup>. Yields were calculated based on nmol reduced C in hydrocarbons per nmol cluster. Experiments that determined the product yields were performed three times (n=6), and data from these experiments are presented as mean±s.d.



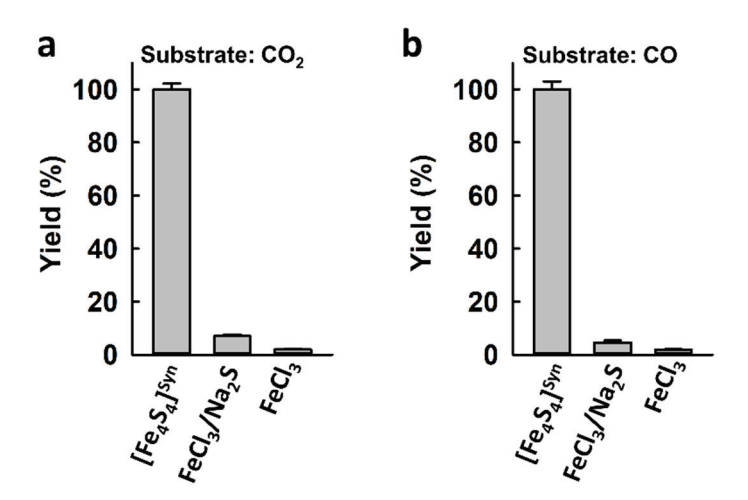
Supplementary Fig. 3 | Redox properties of protein-bound [Fe<sub>4</sub>S<sub>4</sub>] clusters. (a) Yields of CO<sub>2</sub> generated from the oxidation of CO by NifH<sup>Av</sup> or NifH<sup>Ma</sup> in the presence of 20 mM IDS. (b) Titration of the +1/+2 redox couple of the [Fe<sub>4</sub>S<sub>4</sub>] cluster of NifH<sup>Ma</sup>. The oxidation of the cluster from the +1 to the +2 state was monitored by the absorbance at 420 nm. (c) Redox potentials of the +1/+2 couples of the [Fe<sub>4</sub>S<sub>4</sub>] clusters of NifH<sup>Ma</sup> and NifH<sup>Av</sup>. The potential of NifH<sup>Ma</sup> was determined as described in b, and the potential of NifH<sup>Av</sup> was determined in a previous work<sup>2</sup>. The redox titration experiment was performed 3 times, and the representative result is shown in b. Experiments that determined the product yields were performed three times (n=6), and data from these experiments are presented as mean±s.d.



Supplementary Fig. 4 | Reduction of CO to hydrocarbons by protein-bound [Fe<sub>4</sub>S<sub>4</sub>] clusters using dithionite as a reductant. (a) Time-dependent formation of hydrocarbons from CO reduction by NifH<sup>Ma</sup>. (b) Distribution of hydrocarbons generated by NifH<sup>Ma</sup> from the reaction of CO reduction. Experiments that determined the product yields were performed three times (n=6), and data from these experiments are presented as mean±s.d.



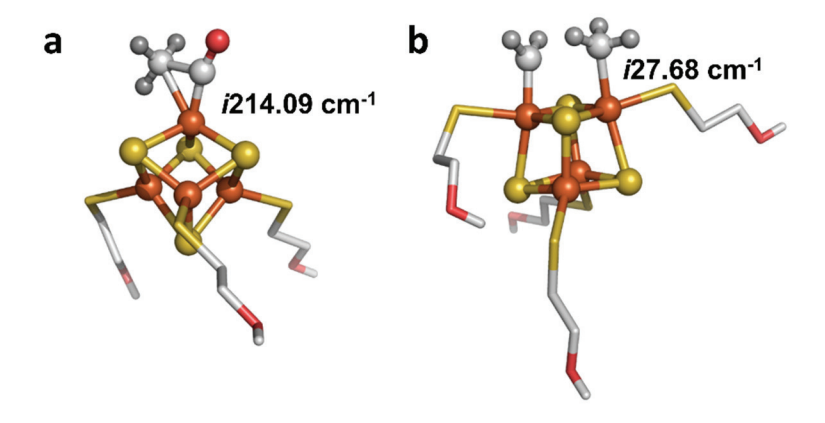
Supplementary Fig. 5 | Structures of protein-bound and synthetic [Fe<sub>4</sub>S<sub>4</sub>] clusters. Shown are x-ray crystal structures of (a) NifH<sup>4ν</sup>-associated [Fe<sub>4</sub>S<sub>4</sub>] cluster with four protein-bound Cys ligands<sup>38</sup> and (b) synthetic [PPh<sub>4</sub>][Fe<sub>4</sub>S<sub>4</sub>(SCH<sub>2</sub>CH<sub>2</sub>OH)<sub>4</sub>] compound (designated [Fe<sub>4</sub>S<sub>4</sub>]<sup>Syn</sup>) with four β-mercaptoethanol thiolate ligands.<sup>39,40</sup> Element colour code: Fe, orange; S, yellow; C, light grey; O, red.



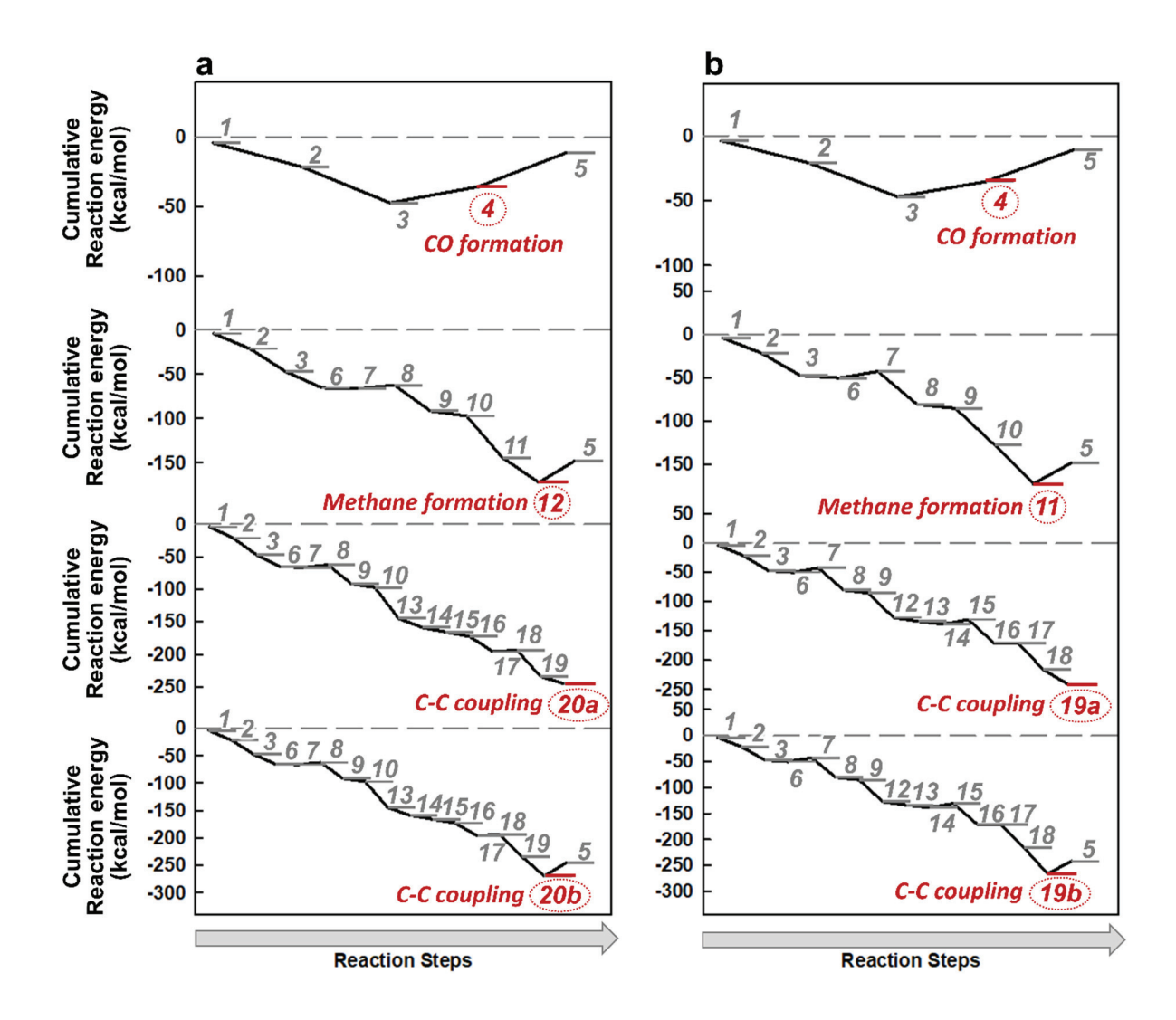
## Supplementary Fig. 6 | Formation of hydrocarbons by [Fe<sub>4</sub>S<sub>4</sub>]<sup>Syn</sup> and Fe-containing controls.

Shown are the percentage yields of hydrocarbons generated from the reduction of (a) CO<sub>2</sub> or (b) CO by [Fe<sub>4</sub>S<sub>4</sub>]<sup>Syn</sup>, or by Fe<sub>3</sub>Cl<sub>3</sub> in the presence and absence of Na<sub>2</sub>S. The experiments were conducted in 20 mM SmI<sub>2</sub>, and the hydrocarbon yield of the [Fe<sub>4</sub>S<sub>4</sub>]<sup>Syn</sup>-based reaction was set as 100%. Experiments that determined the product yields were performed three times (n=6), and data from these experiments are presented as mean±s.d.

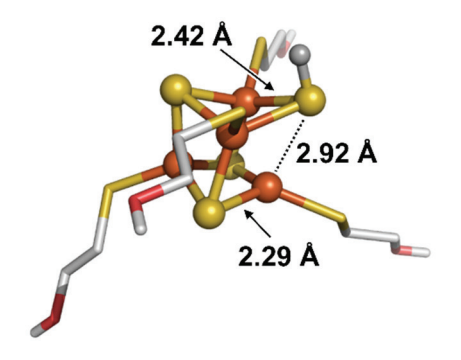
Supplementary Fig. 7 | Structures of the catalyst and proton source for DFT calculations. (a) Lewis Structure of the [Fe<sub>4</sub>S<sub>4</sub>] cluster considered in the computational investigation. (b) Deprotonation reaction of NHEt<sup>+</sup> considered for calculations of all protonation energies.



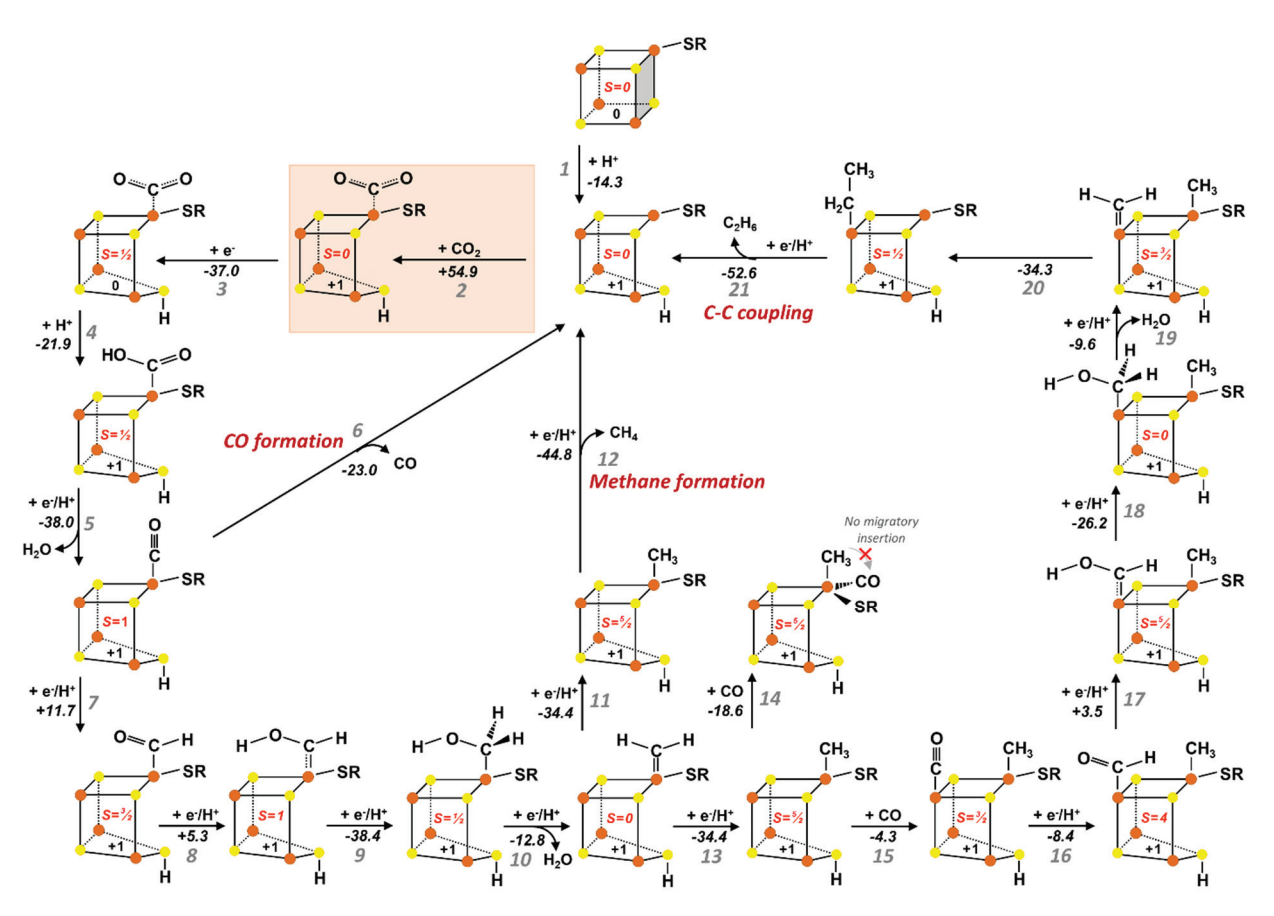
**Supplementary Fig. 8 | Transition states for the proposed mechanisms.** Shown are the transition states (TPSS/def2-TZVP) for (a) migratory insertion (see Fig. 3, step 15) and (b) CH<sub>2</sub>-CH<sub>3</sub> bond formation (see Fig. 4, step 18). Element colour code: Fe, orange; S, yellow; C, light grey; O, red; H, grey.



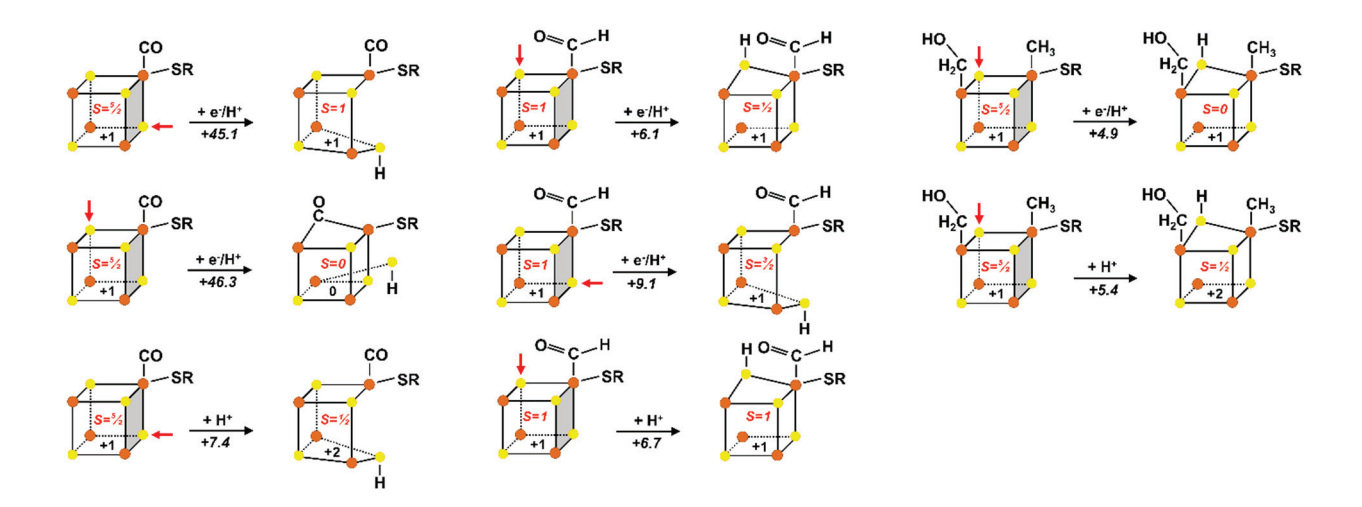
Supplementary Fig. 9 | Cumulative reaction energies of CO<sub>2</sub> reduction pathways catalysed by the [Fe<sub>4</sub>S<sub>4</sub>] cluster. Shown are the energies for the pathways of CO formation, methane formation and C-C coupling that are depicted in (a) Fig. 3 and (b) in Fig. 4. The steps of CO formation, methane formation and C-C coupling are indicated by red circles.



Supplementary Fig. 10 | Protonation of the [Fe<sub>4</sub>S<sub>4</sub>] cluster. Shown is the optimised structure (TPSS/def2-TZVP, COSMO  $\varepsilon$ =37) of the all-ferrous [Fe<sub>4</sub>S<sub>4</sub>] cluster protonated at one of its S atoms. Protonation leads to significant distortion of the cluster and consequently opens up the cubane. Element colour code: Fe, orange; S, yellow; C, light grey; O, red; H, grey.



Supplementary Fig. 11 | Reaction mechanism starting with the protonation of one of the S atoms of the [Fe<sub>4</sub>S<sub>4</sub>] cluster. Reaction energies were derived from the energies of the structurally optimised compounds (TPSS/def2-TZVP, COSMO  $\varepsilon$ =37). Cluster models were considered fully coordinated by SC<sub>2</sub>H<sub>4</sub>OH<sup>-</sup>. Only the ligand of the open Fe site is depicted. SR, SC<sub>2</sub>H<sub>4</sub>OH<sup>-</sup>.



Supplementary Fig. 12 | Examples of endothermic proton or electron/proton transfer reactions to the sulphur atoms of the [Fe<sub>4</sub>S<sub>4</sub>] cluster. Reaction energies were derived from the energies of the structurally optimised compounds (TPSS/def2-TZVP, COSMO  $\varepsilon$ =37). Cluster models were considered fully coordinated by SC<sub>2</sub>H<sub>4</sub>OH<sup>-</sup>. Proton or electron/proton transfer is indicated by a red arrow. Only the ligand of the open Fe site is depicted. SR, SC<sub>2</sub>H<sub>4</sub>OH<sup>-</sup>.

#### **Supplementary References**

- 1. Strop, P. et al. Crystal structure of the all-ferrous [4Fe-4S]<sup>0</sup> form of the nitrogenase iron protein from *Azotobacter vinelandii*. *Biochemistry* **40**, 651–656 (2001).
- 2. Rebelein, J.G., Stiebritz, M.T., Lee, C.C. & Hu, Y. Activation and reduction of carbon dioxide by nitrogenase iron proteins. *Nat. Chem. Biol.* **13**, 147-149 (2017).
- 3. Lowery, T.J. et al. Flavodoxin hydroquinone reduces *Azotobacter vinelandii* Fe protein to the all-ferrous redox state with a S = 0 spin state. *Proc. Natl. Acad. Sci. U. S. A.* **103**, 17131–17136 (2006).
- 4. Lee, C.C., Hu, Y. & Ribbe, M.W. Vanadium nitrogenase reduces CO. Science 329, 642 (2010).
- 5. Hu, Y., Lee, C.C. & Ribbe, M.W. Extending the carbon chain: hydrocarbon formation catalyzed by vanadium/molybdenum nitrogenases. *Science* **333**, 753–755 (2011).
- 6. Yang, Z.Y., Dean, D.R. & Seefeldt, L.C. Molybdenum nitrogenase catalyzes the reduction and coupling of CO to form hydrocarbons. *J. Biol. Chem.* **286**, 19417-19421 (2011).
- 7. Lee, C.C., Hu, Y. & Ribbe, M.W. ATP-independent formation of hydrocarbons catalyzed by isolated nitrogenase cofactors. *Angew. Chem. Int. Ed.* **51**, 1947–1949 (2012).
- 8. Lee, C.C, Hu, Y. & Ribbe, M.W. Catalytic reduction of CN<sup>-</sup>, CO, and CO<sub>2</sub> by nitrogenase cofactors in lanthanide-driven reactions. *Angew. Chem. Int. Ed.* **54**, 1219–1222 (2015).
- 9. Hu, Y. & Ribbe, M.W. Nitrogenases—A tale of carbon atom(s). *Angew. Chem. Int. Ed. 55*, 8216–8226 (2016).
- 10. Tanifuji, K. et al. Structure and reactivity of an asymmetric synthetic mimic of nitrogenase cofactor. *Angew. Chem. Int. Ed.* **55**, 15633–15636 (2016).
- 11. Rao, P.V. & Holm, R.H. Synthetic analogues of the active sites of iron–sulfur proteins. *Chem. Rev.* **104**, 527–560 (2004).
- 12. Lee, S.C. & Holm, R.H. The clusters of nitrogenase: synthetic methodology in the construction of weak-field clusters. *Chem. Rev.* **104**, 1135–1157 (2004).
- 13. Ohta, S. & Ohki, Y. Impact of ligands and media on the structure and properties of biological and biomimetic iron-sulfur clusters. *Coord. Chem. Rev.* **338**, 207–225 (2017).
- 14. McMillan, R.S., Renaud, J., Reynolds, J.G. & Holm, R.H. Biologically related iron-sulfur clusters as reaction centers. Reduction of acetylene to ethylene in systems based on [Fe<sub>4</sub>S<sub>4</sub>(SR)<sub>4</sub>]<sup>3-</sup>. *J. Inorg. Biochem.* **11**, 213–227 (1979).
- 15. Coucouvanis, D. et al. The catalytic reduction of hydrazine to ammonia by the MoFe<sub>3</sub>S<sub>4</sub> cubanes and implications regarding the function of nitrogenase. Evidence for direct involvement of the molybdenum atom in substrate reduction. *J. Am. Chem. Soc.* 115: 12193–12194 (1993).
- 16. Malinak, S.M., Demadis, K.D. & Coucouvanis, D. Catalytic reduction of hydrazine to ammonia by the VFe<sub>3</sub>S<sub>4</sub> cubanes. Further evidence for the direct involvement of the heterometal in the reduction of nitrogenase substrates and possible relevance to the vanadium nitrogenases. *J. Am. Chem. Soc.* **117**, 3126–3133 (1995).
- 17. Komeda, N., Nagao, H., Matsui, T., Adachi, G. & Tanaka, K. Electrochemical carbon dioxide fixation to thioesters catalyzed by molybdenum-iron-sulfur cluster [Mo<sub>2</sub>Fe<sub>6</sub>S<sub>8</sub>(SEt)<sub>9</sub>]<sup>3-</sup>. *J. Am. Chem. Soc.* **114**, 3625–3630 (1992).
- 18. Christou, G., Holm, R.H., Sabat, M. & Ibers, J.A. A hexanuclear iron-sulfide-thiolate cluster: assembly and properties of [Fe<sub>6</sub>S<sub>9</sub>(S-*t*-C<sub>4</sub>H<sub>9</sub>)<sub>2</sub>]<sup>4-</sup> containing three types of bridging sulfur atoms. *J. Am. Chem. Soc.* **103**, 6269-6271(1981).

- 19. Sickerman, N.S. et al. Reduction of C1 substrates to hydrocarbons by the homometallic precursor and synthetic mimic of the nitrogenase cofactor. *J. Am. Chem. Soc.* **139**, 603–606 (2017).
- 20. Huber, C. & Wächtershäuser, G. Activated acetic acid by carbon fixation on (Fe,Ni)S under primordial conditions. *Science* **276**, 245–247 (1997).
- 21. Scheidler, C., Sobotta, J., Eisenreich, W., Wächtershäuser, G. & Huber, C. Unsaturated C3,5,7,9-monocarboxylic acids by aqueous, one-pot carbon fixation: possible relevance for the origin of life. *Sci. Rep.* **6**, 27595 (2016).
- 22. Huber, C. & Wächtershäuser, G. Alpha-Hydroxy and alpha-amino acids under possible Hadean, volcanic origin-of-life conditions. *Science* **314**, 630–632 (2006).
- 23. Huber, C. & Wächtershäuser, G. Peptides by activation of amino acids with CO on (Ni,Fe)S surfaces: implications for the origin of life. *Science* **281**, 670–672 (1998).
- 24. Wächtershäuser, G. On the chemistry and evolution of the pioneer organism. *Chem. Biodivers.* **4**, 584–602 (2007).
- 25. Roslev, P., Iversen, N. & Henriksen, K. Oxidation and assimilation of atmospheric methane by soil methane oxidizers. *Appl. Environ Microbiol.* **63**, 874–880 (1997).
- 26. Coleman, N.V. & Spain, J.C. Distribution of the coenzyme M pathway of epoxide metabolism among ethene- and vinyl chloride-degrading Mycobacterium strains. *Appl. Environ. Microbiol.* **69**, 6041–6046 (2003).
- 27. Glikson, A.Y. Milestones in the evolution of the atmosphere with reference to climate change. *Aust. J. Earth Sci.* **55**, 125–139 (2008).
- 28. Rebelein, J.G., Lee, C.C., Hu, Y. & Ribbe, M.W. The *in vivo* hydrocarbon formation by vanadium nitrogenase follows a secondary metabolic pathway. *Nat. Commun.* 7, 13641 (2016).
- 29. Lu, X.B., Ren, W.M. & Wu, G.P. CO<sub>2</sub> copolymers from epoxides: catalyst activity, product selectivity, and stereochemistry control. *Acc. Chem. Res.* **45**, 1721–1735 (2012).
- 30. Martín, C., Fiorani, G. & Kleij, A.W. Recent advances in the catalytic preparation of cyclic organic carbonates. *ACS Catal.* **5**, 1353–1370 (2015).
- 31. Wu, X.F. et al. Transition-metal-catalyzed carbonylation reactions of olefins and alkynes: a personal account. *Acc. Chem. Res.* **47**, 1041–1053 (2014).
- 32. Shima, T. & Hou, Z. Hydrogenation of carbon monoxide by tetranuclear rare earth metal polyhydrido complexes. Selective formation of ethylene and isolation of well-defined polyoxo rare earth metal clusters. *J. Am. Chem. Soc.* **128**, 8124–8125 (2006).
- 33. Dry, M.E. The Fischer–Tropsch process: 1950–2000. Catal. Today 71, 227–241 (2002).
- 34. Zhang, Q., Cheng, K., Kang, J., Deng, W. & Wang, Y. Fischer-Tropsch catalysts for the production of hydrocarbon fuels with high selectivity. *ChemSusChem.* 7, 1251–1264 (2014).
- 35. Khodakov, A.Y., Chu, W. & Fongarland, P. Advances in the development of novel cobalt Fischer-Tropsch catalysts for synthesis of long-chain hydrocarbons and clean fuels. *Chem. Rev.* **107**, 1692–1744 (2007).
- 36. Kortlever, R., Shen, J., Schouten, K.J.P., Calle-Vallejo, F. & Koper, M.T.M. Catalysts and reaction pathways for the electrochemical reduction of carbon dioxide. *J. Phys. Chem. Lett.* **6**, 4073–4082 (2015).
- 37. Zhu, D.D., Liu, J.L. & Qiao, S.Z. Recent advances in inorganic heterogeneous electrocatalysts for reduction of carbon dioxide. *Adv. Mater.* **28**, 3423–3452 (2016).

- 38. Georgiadis, M.M. et al. Crystallographic structure of the nitrogenase iron protein from *Azotobacter vinelandii*. *Science* **257**, 1653–1659 (1992).
- 39. Averill, B.A., Herskovitz, T., Holm, R.H. & Ibers, J.A. Synthetic analogs of the active sites of iron-sulfur proteins. II. Synthesis and structure of the tetra(mercapto-μ<sub>3</sub>-sulfido-iron) clusters, (Fe<sub>4</sub>S<sub>4</sub>(SR)<sub>4</sub>)<sup>2</sup>-. *J. Am. Chem. Soc.* **95**, 3523–3534 (1973).
- 40. Barclay, J.E., Davies, S.C., Evans, D.J., Hughes, D.I. & Longhurst, S. Lattice effects in the Mössbauer spectra of salts of  $[Fe_4S_4\{S(CH_2)_nOH\}_4]^{2-}$ . Crystal structures of  $[PPh_4]_2[Fe_4S_4\{S(CH_2)_nOH\}_4]$  (n=2, 3 and 4). Inorg. Chim. Acta. **291**, 101–108 (1999).